

# Timing and Origin of Compressional Tectonism in Mare Tranquillitatis

T. Frueh<sup>1</sup>, H. Hiesinger<sup>1</sup>, C. H. van der Bogert<sup>1</sup>, J. D. Clark<sup>2</sup>, T. R. Watters<sup>3</sup>, and N. Schmedemann<sup>1</sup>

<sup>1</sup>Institut für Planetologie, Westfälische Wilhelms-Universität Münster, Münster, Germany, <sup>2</sup>School of Earth and Space Exploration, Arizona State University, Tempe, AZ, USA, <sup>3</sup>Center of Earth and Planetary Studies, National Air and Space Museum, Smithsonian Institution, Washington, DC, USA

## Key Points:

- Early compressional tectonism in Tranquillitatis, in the form of wrinkle ridges, is presumably related to subsidence and basin loading
- Later tectonism could reflect the evolution from a basin-localized to a global stress field and the continued growth of ancient faults
- Recent wrinkle ridge and lobate scarp formation in Tranquillitatis occurred in the last 50 Ma and is influenced by a global stress field

## Supporting Information:

Supporting Information may be found in the online version of this article.

## Correspondence to:

T. Frueh,  
[thomas.frueh@uni-muenster.de](mailto:thomas.frueh@uni-muenster.de)

## Citation:

Frueh, T., Hiesinger, H., van der Bogert, C. H., Clark, J. D., Watters, T. R., & Schmedemann, N. (2023). Timing and origin of compressional tectonism in Mare Tranquillitatis. *Journal of Geophysical Research: Planets*, 128, e2022JE007533. <https://doi.org/10.1029/2022JE007533>

Received 17 AUG 2022

Accepted 20 JAN 2023

© 2023. The Authors.

This is an open access article under the terms of the [Creative Commons Attribution License](#), which permits use, distribution and reproduction in any medium, provided the original work is properly cited.

**Abstract** The lithosphere of the Moon has been deformed by tectonic processes for at least 4 billion years, resulting in a variety of tectonic surface features. Extensional large lunar graben formed during an early phase of net thermal expansion before 3.6 Ga. With the emplacement of mare basalts at ~3.9–4.0 Ga, faulting and folding of the mare basalts initiated, and wrinkle ridges formed. Lunar wrinkle ridges exclusively occur within the lunar Maria and are thought to be the result of superisostatic loading by dense mare basalts. Since 3.6 Ga, the Moon is in a thermal state of net contraction, which led to the global formation of small lobate thrust faults called lobate scarps. Hence, lunar tectonism recorded changes in the global and regional stress fields and is therefore an important archive for the thermal evolution of the Moon. Here, we mapped tectonic features in the non-mascon basin Mare Tranquillitatis and classified these features according to their respective erosional states. This classification aims to provide new insights into the timing of lunar tectonism and the associated stress fields. We found a wide time range of tectonic activity, ranging from ancient to recent (3.8 Ga to <50 Ma). Early wrinkle ridge formation seems to be closely related to subsidence and flexure. For the recent and ongoing growth of wrinkle ridges and lobate scarps, global contraction with a combination of recession stresses and diurnal tidal stresses, as well as with a combination of South Pole-Aitken ejecta loading and true polar wander are likely.

**Plain Language Summary** The lithosphere of the Moon has been deformed by tectonic processes for at least 4 billion years, resulting in a variety of tectonic surface features. Simple compressional asymmetric landforms are called lobate scarps and complex compressional features, which form as a result of the combination of faulting and folding, are known as wrinkle ridges. Lunar wrinkle ridges only occur within the lunar Maria. It has been argued that their formation is linked to the subsidence of the dense mare basalts, which would have happened in the early history of the Moon. We mapped all of these features within a dark lunar region called Mare Tranquillitatis and then studied their morphology on high-resolution images. Based on their morphology, we found a wide time range of tectonic activity, ranging from ancient to recent. Large wrinkle ridges seem to be ancient and influenced by subsidence. Smaller wrinkle ridges and lobate scarps show signs of recent activity. They likely formed recently within the last hundred million years because of the Moon's current state of global compression.

## 1. Introduction

The Moon's surface hosts a variety of extensional and compressional tectonic features, which recorded the history of the acting regional and global stress systems. Compressional tectonism was initiated with the emplacement of the mare basalts and the shift of net global extension to net global contract at ~3.6 Ga, which led to the formation of the two major compressional tectonic landforms: lobate scarps and wrinkle ridges (Fagin et al., 1978; Lucchitta & Watkins, 1978; Solomon & Head, 1979; Watters & Johnson, 2009; Wilhelms et al., 1987). Lobate scarps are the surface expressions of simple thrust faults and are the dominating tectonic landforms in the lunar highlands (Binder & Gunga, 1985; Watters & Johnson, 2009; Watters et al., 2010). Lunar wrinkle ridges exclusively occur in the Maria or basalt-covered regions and are a result of a complex interaction between thrust faulting and folding (Lucchitta, 1976; Schultz, 2000; Wilhelms et al., 1987). The compressional tectonism in the Maria is thought to have originated from the superisostatic loading by dense mare basalts and the flexure of the lithosphere (Freed et al., 2001). This model has been established for the mascon (mass concentrations) Maria, like Mare Imbrium or Mare Serenitatis. However, not all lunar Maria are

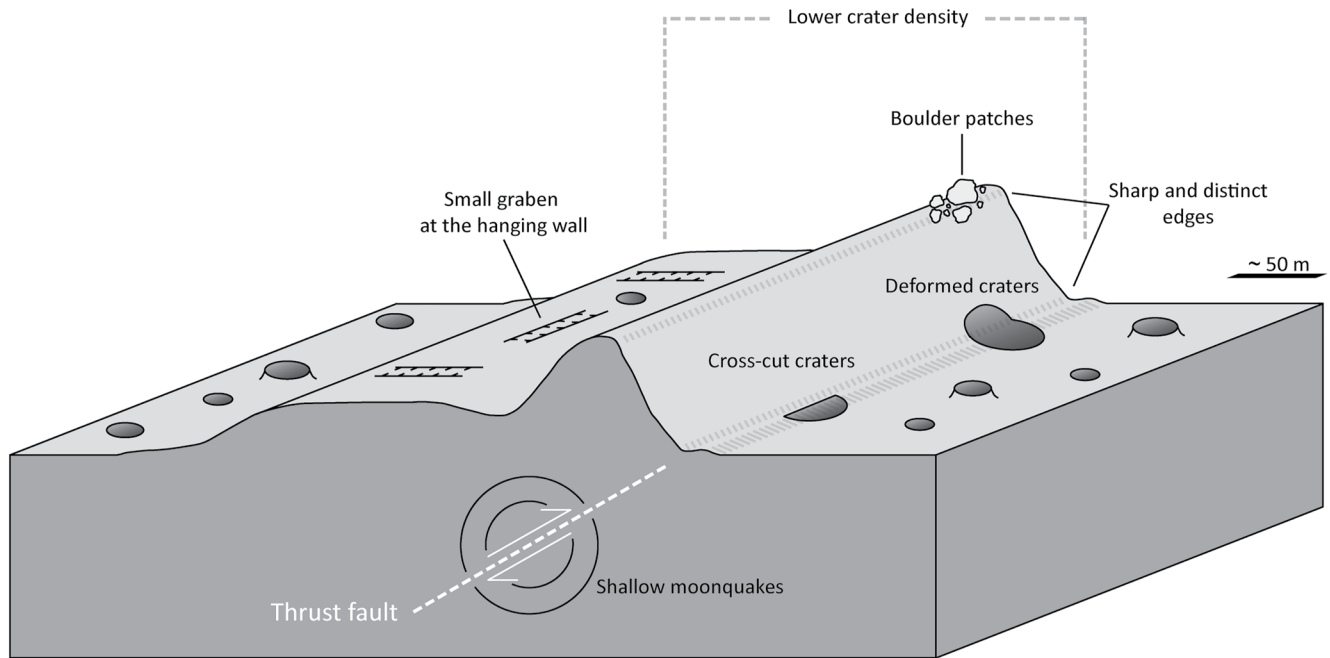


**Figure 1.** The schematic model of the signs of recent tectonic activity of surface features. A small crisp wrinkle ridge segment in Mare Tranquillitatis served as a template for the topographic profile. The signs of recent tectonic activity apply, however, for both lobate scarps and wrinkle ridges. These signs include crisp morphology, deformed craters, cross-cut craters, small graben and troughs, lower crater density, and boulder fields/patches. In this study, the boulder abundance was not used to determine the degradational stage of a wrinkle ridge or lobate scarp. Shallow moonquakes detected by the Apollo missions have been previously correlated with the activity of lobate scarps.

considered to be mascons because they lack the strong positive gravitational signal of mascon basins (Muller & Sjogren, 1968). The stress systems of those non-mascon basins are less well understood and still a matter of discussion.

Furthermore, the acting stress fields changed with time, and the age of tectonic landforms, therefore, contains important information on the stresses triggering their formation. Most of the deformation of the Maria is thought to have occurred early in lunar history (e.g., Fagin et al., 1978; Ono et al., 2009; Watters & Johnson, 2009; Yue et al., 2017). However, recent studies have uncovered young tectonic features in the lunar highlands and Maria, including young and recently active wrinkle ridges (e.g., Lu et al., 2019; Nypaver & Thomson, 2022; Valantinas & Schultz, 2020; Watters et al., 2010; Williams et al., 2019). The young landforms exhibit distinctive morphological features, such as steep slopes, sharp edges, a crisp appearance, crosscutting relationships with craters, and the occurrence of small crisp graben in their close vicinity (Figure 1). The trigger behind this recent tectonic activity is also still a matter of discussion.

Mare Tranquillitatis, which was the stage of the first human landing site as part of the Apollo 11 mission, is one of those non-mascon basins. Mare Tranquillitatis is an irregularly shaped basin (Figure 2), consisting of a deep and deeply basalt-filled western part and a shallow and shallow-filled eastern part (De Hon, 1974, 2017; Dvorak & Phillips, 1979; Konopliv et al., 2001; Zuber et al., 2013). The western part is associated with intensive deformation and circular, radial, and NS trending wrinkle ridge patterns, while the eastern part experienced less deformation and exhibits loose wrinkle ridge patterns. In addition to wrinkle ridges, lobate scarps, graben, and a large normal fault (called Rupes Cauchy) are present in the mare. A study by Yue et al. (2017), discovered an unusually young average age of  $\sim 2.4$  Ga of large wrinkle ridges in Mare Tranquillitatis relative to wrinkle ridges in other Maria. The reason behind this discrepancy remains unknown.

This study aims to contribute to the discussion on the age of tectonic landforms, stress systems of non-mascon Maria, and the trigger behind the recent tectonic activity. To achieve this goal, we created a tectonic map of Mare Tranquillitatis and studied the degradational state of compressional tectonic features to gain age information. By combining the tectonic analysis with the age of the tectonic features, we aim to uncover the evolution of the stress field acting in Mare Tranquillitatis.

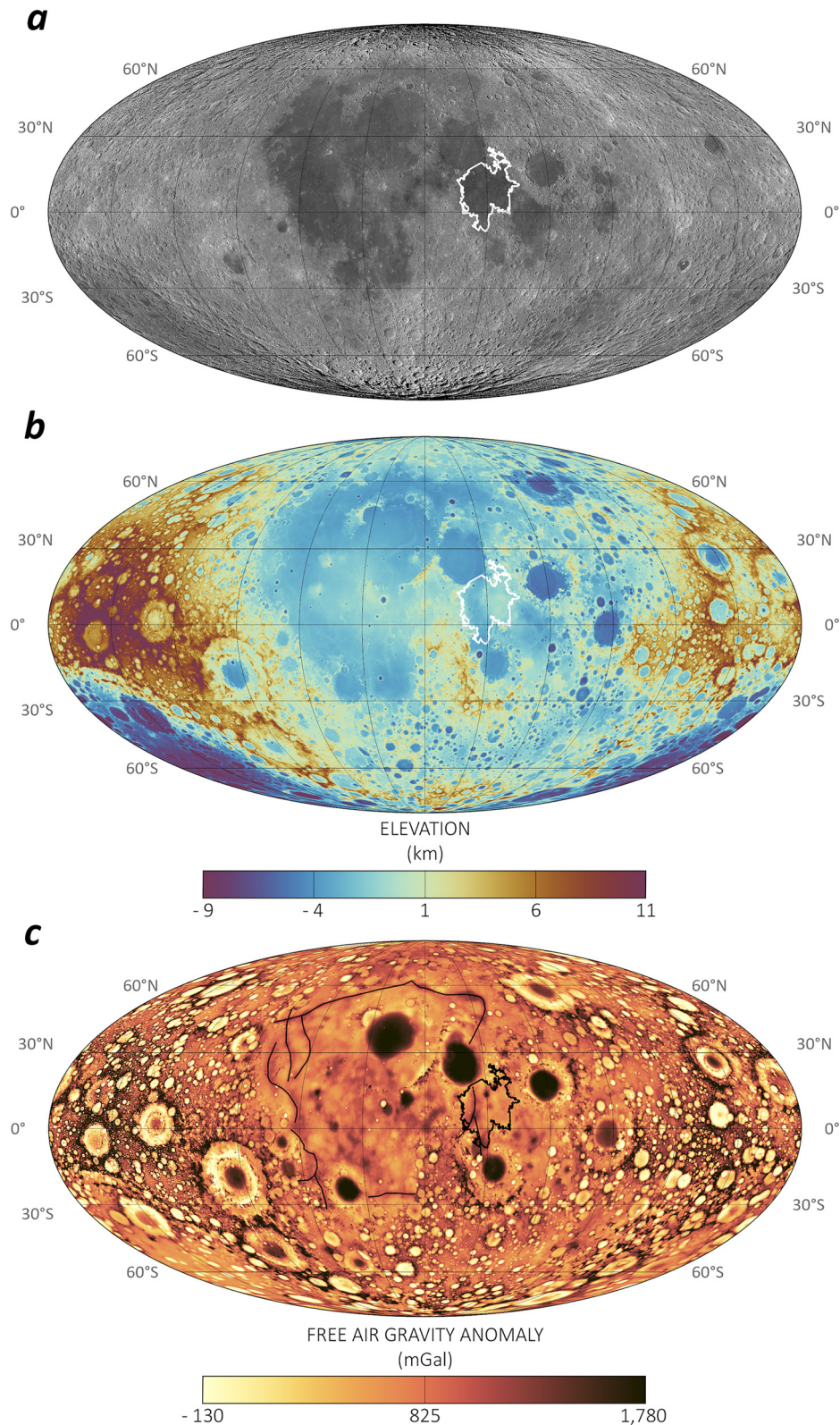


**Figure 2.** (a) Location of Mare Tranquillitatis (white outline; Nelson et al., 2014) near the lunar equator projected onto the global merged WAC mosaic. (b) Mare Tranquillitatis (black outline) projected onto the LRO LOLA—SELENE Kaguya DEM (Barker et al., 2016; Neumann, 2009). (c) The black outline of Mare Tranquillitatis projected onto the GRAIL Free Air Gravity map (Kahan, 2013; harmonic degree and order of 660). The black lines sketch the proposed quasi-rectangular pattern of ancient intrusion (after Andrews-Hanna et al., 2013).

## 2. Background

### 2.1. Lunar Tectonics

The tectonic history of the Moon began with a period of net thermal expansion, which is argued to have shifted to net contraction around 3.6 Ga (Lucchitta & Watkins, 1978). Since then, global cooling has induced a dominantly contractional global stress field (Solomon & Head, 1979; Watters & Johnson, 2009; Wilhelms et al., 1987). This shift in the thermal state of the Moon is preserved in its tectonic landforms. Large-scale crustal extension and thus the formation of large lunar graben ended at  $\sim 3.6$  Ga (Lucchitta & Watkins, 1978; Watters & Johnson, 2009). Following the shift, compressional features, that is, lobate scarps, became the dominant globally forming tectonic landforms. The emplacement of the mare basalts started at  $\sim 3.9$ – $\sim 4.0$  Ga and generally ceased at  $\sim 1.2$  Ga (Hiesinger et al., 2011). With the main period of basalt emplacement at about 3.6–3.8 Ga (Hiesinger et al., 2011), the formation of wrinkle ridges began (Fagin et al., 1978; Watters, 1988; Watters & Johnson, 2009).

Wrinkle ridges are common contractional tectonic features on the Moon, Mercury, Mars, and Venus (Golombek et al., 1991; Plescia & Golombek, 1986; Watters, 1988; Watters & Johnson, 2009). On the Moon, wrinkle ridges exclusively occur within the mare basins (Lucchitta, 1976; Watters & Johnson, 2009; Wilhelms et al., 1987) to which they typically appear radial and concentric (Watters & Johnson, 2009; Whitaker, 1981). They typically show an asymmetric profile and consist of a broad arch and a superimposed irregular ridge (Plescia & Golombek, 1986; Strom, 1972; Watters, 1988), but their morphology is highly variable (Plescia & Golombek, 1986; Watters, 1988). Wrinkle ridges reach up to 300 km in length and 20 km in width (Sharpton & Head, 1988). Often one flank of the wrinkle ridge, the vergent side, has a steeper slope than the other, but this asymmetry can reverse along the wrinkle ridge. The superposed ridge is usually located near the steeper flank of the arch (Plescia & Golombek, 1986; Watters, 1988). However, both structures can occur independently from one another (Watters & Johnson, 2009). Wrinkle ridge segments often occur in en-echelon arrangements (Watters & Johnson, 2009). Smaller secondary or tertiary ridges occur near or on top of larger primary ridges (Watters, 1988; Watters & Johnson, 2009). The surface texture of wrinkle ridges often resembles a crisscross “elephant-hide” structure (Gold, 1972). Elephant-hide structures can be found on slopes everywhere on the Moon and are thought to form due to regolith creep and seismic shaking (Bondarenko et al., 2022; Zharkova et al., 2020).

Since wrinkle ridges deform even young mare basalts with an age of  $\sim 1.2$  Ga, crustal shortening associated with lunar Maria occurred at least as recently as  $\sim 1.2$  Ga (Watters & Johnson, 2009). A global survey of possible formation times found average ages  $>3.0$  Ga for large wrinkle ridge structures (Yue et al., 2017). Wrinkle ridges in Mare Tranquillitatis, however, appear to be younger with an average age of  $\sim 2.4$  Ga (McGovern et al., 2022; Yue et al., 2017).

While the exact kinematics of wrinkle ridge formation are still debated, the formation is generally explained by a combination of thrusting and folding (Schultz, 2000; Watters & Johnson, 2009). Hence, wrinkle ridges can be interpreted as anticlinal structures above a non-surface breaking blind thrust fault (Schultz, 2000; Watters & Johnson, 2009). For these processes to occur, a layered stratigraphy of the mare basalts is necessary (Schultz, 2000). The fault geometry may be planar or listric, there may be single or multiple faults, and the depth of faulting may be shallow or deep (i.e., thick- or thin-skinned deformation; Montési & Zuber, 2003; Okubo & Schultz, 2003, 2004; Schultz, 2000; Watters, 2004, 2022). The wrinkle ridge formation is thought to be the result of superisostatic loading by dense mare basalts inducing subsidence and flexure of the lithosphere (i.e., mascon tectonics; Byrne et al., 2015; Freed et al., 2001; Schleicher et al., 2019). This led to compressional stresses in the basin center and extensional stresses at the basin margins, and consequently, in basin concentric and radial wrinkle ridges (Freed et al., 2001). It is also suggested that global cooling instead of subsidence was the dominant cause of wrinkle ridge formation after 3.55 Ga onwards (Ono et al., 2009; Watters & Johnson, 2009). Another proposed influence on the global stress field and wrinkle formation is deep transient stresses generated by the South Pole-Aitken (SPA) basin (Schultz & Crawford, 2011). This model predicts antipodal failures on the lunar nearside due to extensions deep within the Moon, which would have reactivated deep-seated faults. Wrinkle ridge patterns of the lunar nearside do spatially correlate with wrinkle ridge patterns predicted by this model (Schultz & Crawford, 2011; Valantinas & Schultz, 2020). GRAIL Bouguer gravity gradient data revealed a possible quasi-rectangular pattern of ancient deep rift valleys that are proposed to influence the localization of some wrinkle ridges (Figure 2; Andrews-Hanna et al., 2014). The wrinkle ridge formation might therefore be a result of an interplay of various factors on the regional and global stress fields, which will be discussed later.

Lobate scarps are linear to curvilinear small-scaled compressional structures, which mainly occur in the lunar highlands. They are asymmetric with a steeply sloping scarp face and a gently sloping back scarp. The direction of the scarp face often reverses along the strike (Binder & Gunga, 1985; Watters & Johnson, 2009; Watters et al., 2010). In contrast to wrinkle ridges, they are thought to result from shallow surface-breaking thrust faults (Watters & Johnson, 2009). In some cases, wrinkle ridges transform into lobate scarps at mare highland boundaries (Clark et al., 2019; Lucchitta, 1976; Watters & Johnson, 2009; Watters et al., 2010). Lobate scarps are thought to be among the youngest tectonic features on the Moon (e.g., Binder & Gunga, 1985; van der Bogert et al., 2018; Watters & Johnson, 2009; Watters et al., 2010; Watters et al., 2019). Binder and Gunga (1985) suggested that highland scarps are younger than 1 Ga. Crater size-frequency distribution (CSFD) measurements of lobate scarps support late Copernican ages (van der Bogert et al., 2018). From the infilling rates of small-scale back-scarp graben, the age of some lobate scarps might be <50 Ma (Watters et al., 2012).

Recent studies revealed fresh activity of wrinkle ridges and lobate scarps (e.g., Lu et al., 2019; Nypaver & Thomson, 2022; Valantinas & Schultz, 2020; Watters et al., 2010; Williams et al., 2019). The evidence includes for both landforms (Figure 1), the abundance of boulder fields and patches (French et al., 2019; Valantinas & Schultz, 2020; Watters et al., 2019), a distinct crisp morphology (e.g., Watters et al., 2010; Williams et al., 2019), crosscutting of impact craters (Lu et al., 2019; Nypaver & Thomson, 2022; Watters et al., 2010), ages <1 Ga determined from CSFD methods (Lu et al., 2019; Valantinas et al., 2018; van der Bogert et al., 2018), shallow moonquakes (Watters et al., 2019), boulder falls (Senthil Kumar et al., 2016), and associated small meter-scaled graben (French et al., 2015; Valantinas & Schultz, 2020; Watters et al., 2012). The correlation between boulder falls and seismic activity, however, has been questioned recently (Bickel et al., 2021; Ikeda et al., 2022), highlighting the ongoing and early state of the study of recent tectonic activity. Late-stage global contraction is consistent with both an initially molten Moon (Binder & Gunga, 1985; Watters et al., 2019) and a near-surface magma ocean (Solomon, 1986; Solomon & Head, 1979; Watters et al., 2019), however, the magnitude of the late-stage stresses predicted in the totally molten Moon model is inconsistent with the population of small lobate thrust fault scarps (Watters et al., 2012, 2015). The global contraction would result in scarps with random orientations (Watters et al., 2015, 2019). However, since scarp orientations are non-randomly distributed, Watters et al. (2015, 2019) proposed a significant contribution of tidal stresses in the current stress state on the Moon. These stresses might also have an important influence on recent wrinkle ridge formation and activity (Williams et al., 2019). A model including SPA ejecta loading, true polar wander, and global contraction is also able to reproduce the observed scarp distribution (Matsuyama et al., 2021). Valantinas and Schultz (2020) proposed that active wrinkle ridges are part of an active nearside tectonic system (ANTS), resulting from the fault adjustment of ancient deep-seated intrusions, which were reactivated by the SPA forming impact. Deep moonquakes could be possible signs of those readjustments (Valantinas & Schultz, 2020). However, stresses related to these ancient sources of activity may have largely relaxed long ago and further models are needed to quantify their influence on today's global stress field.

## 2.2. Mare Tranquillitatis

Mare Tranquillitatis is centered at 8.35°N and 30.83°E, and extends over approximately 875 km in diameter (Figure 2). In the northwest, it borders Mare Serenitatis and Mare Fecunditatis in the southeast. Mare Tranquillitatis is irregularly shaped and dividable into two regions. The eastern part has a higher topographic elevation of up to −350 m (Figure 2). The western region has a lower elevation below −2,000 km. The somewhat irregular shape of Tranquillitatis does not resemble the typical circular mare basin shape (e.g., Mare Imbrium, Mare Serenitatis, or Mare Crisium).

Mare Tranquillitatis is a non-mascon basin of pre-Nectarian age (Wilhelms et al., 1987). The mare fills at least one multi-ring basin (De Hon, 1974; Spudis, 1993), but a second overlapping basin is possible (Bhatt et al., 2020; De Hon, 2017). The mare basalts of Mare Tranquillitatis are of Imbrian age of 3.39–4.23 Ga (Hiesinger et al., 2000, 2011). Most of the basalts show a CSFD age of 3.6–3.7 Ga (Hiesinger et al., 2000). These ages agree with the radiometric age of 3.67 Ga of the returned Apollo 11 samples (Hiesinger et al., 2000; Iqbal et al., 2019; Wilhelms et al., 1987). The western part of Mare Tranquillitatis is slightly younger than the eastern part (Hiesinger et al., 2000, 2011). Crustal thickness varies from west to east as well. With a thickness between 10 and 30 km, the crust is thinnest in the west. This agrees with the free air data, which indicate a positive gravity anomaly in the western region (Figure 2; Zuber et al., 2013). This gravitational anomaly suggests a

trough-like structure connecting Mare Tranquillitatis with Mare Nectaris in the south and Mare Serenitatis in the north (De Hon, 1974). Recent publications suggest that this trough is part of a system of deep-seated intrusions that form a rectangular pattern on the near side of the Moon (Andrews-Hanna et al., 2014; Valantinas & Schultz, 2020). The deepest basalt-filled regions of the trough in Mare Tranquillitatis are the Lamont region and a structure near the Torricelli crater (De Hon, 1974, 2017; Dvorak & Phillips, 1979; Konopliv et al., 2001; Zuber et al., 2013). The Lamont region represents a circular positive free air anomaly in the southwest of Tranquillitatis and is superficially recognizable as a circular ring of wrinkle ridges and an overall topographic low (Dvorak & Phillips, 1979; Scott, 1974). It has been interpreted to be either a buried impact crater or ghost crater (Dvorak & Phillips, 1979; Scott, 1974) or a feature of volcanic origin (Zhang et al., 2018). Several large graben occur throughout the mare, but most of them occur in the western region of Mare Tranquillitatis. The large graben Rima Cauchy and a parallel normal fault called Rupes Cauchy occur in eastern Mare Tranquillitatis (Bhatt et al., 2020). Many smaller volcanic domes and cones are abundant in the eastern mare (Qiao et al., 2020; Spudis et al., 2013). Spudis et al. (2013) proposed two large shield volcano-like structures in eastern Mare Tranquillitatis as an explanation for the abundance of volcanic features. Mare Tranquillitatis has the largest abundance of irregular mare patches, which were interpreted to be evidence of volcanism within the past 100 Ma (Braden et al., 2014; Qiao et al., 2020).

### 3. Data and Methods

In this study, a tectonic map and a tectonic feature map of Mare Tranquillitatis and the adjacent highlands were created using ESRI's ArcGIS version 10.5.1 and ArcGIS Pro. Wrinkle ridges and lobate scarps typically consist of a variable number of individual segments. In the tectonic map, for example, a wrinkle ridge consisting of several individual segments is represented by one continuous polyline. This map was used for the tectonic analysis. For the feature map, we mapped the individual segments for morphological analysis, because individual segments might have varying formation ages. Both maps were created on Kaguya TC images (pixel scale of ~10 m; Ohtake et al., 2008) at a scale of 1:80,000. To achieve complete coverage of Mare Tranquillitatis, 84 TC tiles of both west and east illumination maps were integrated into the ArcGIS environment. Topographic information was gathered from the merged LRO LOLA—SELENE Kaguya Digital Elevation Model (DEM; Barker et al., 2016). Hillshade maps with different azimuth and height combinations, as well as slope maps were derived from this DEM.

For the tectonic map, features were classified as wrinkle ridges, lobate scarps, and unidentified. Unidentified features are linear positive topographic features with a possible but unproven tectonic origin (other possible origins are, e.g., dikes, lava flows, surface expressions of buried structures, or ejecta remnants). Additionally, we mapped extensional features, that is, graben and the normal fault segments of Rupes Cauchy for complete coverage of the tectonic setting of Mare Tranquillitatis and for the following tectonic analysis. The polylines of wrinkle ridges were drawn at the center of the anticline. Since the morphology of wrinkle ridges is highly variable, Kaguya TC images, topographical data, slope maps, and hillshade maps were used to identify wrinkle ridge structures. A wrinkle ridge was mapped if it exhibited the classical morphological characteristics (as described in Section 2.1) or showed a distinguishable asymmetric change in slope and topography. For lobate scarps and normal faults, the polylines were drawn at the scarp face base and for graben, the polylines were drawn at the graben center.

For the feature map, we focused on Kaguya TC images to identify individual features of wrinkle ridges and lobate scarps. Polylines were drawn on top of each wrinkle ridge crest. Every polyline represents a continuous wrinkle ridge crest segment. A new polyline was drawn if the orientation of the wrinkle ridge changes or if the crest segment is interrupted. Since mapping took place on the 1:80,000 scale, smaller structures are mostly represented by a single polyline. If no crest could be visibly identified, the edge of the steeper side was used for mapping. Lobate scarps features were mapped at the scarp face base. The morphology of each of these mapped features was then examined on Narrow Angle Camera (NAC) images in Quickmap and ArcGIS, with incidence angles of between 55° and 90°. Each wrinkle ridge segment was classified according to their respective appearances and erosional states into the classes crisp, moderately degraded, advanced degraded, and heavily degraded (similar to Williams et al., 2019). Attention was paid to their general appearance, the number of crosscut and superimposed craters, and to small associated graben (Table 1). The boulder abundance was not used in the classification, because we wanted to compare our results with the previously published boulder abundance maps (French et al., 2019; Valantinas & Schultz, 2020).

**Table 1**  
*Characteristics Used for the Classification of the Erosional States of Wrinkle Ridges and Lobate Scarps*

Class	Morphology	Crater crosscutting	Graben
Crisp	Features with sharp and morphologically distinct edges and steep slopes.	Can crosscut and deform craters with diameter ranges of <50–100 m.	Small (width <50 m) and crisp clusters of graben are present.
Moderately degraded	Features with slightly rounded edges and steep to moderate slopes.	Can crosscut and deform craters with, generally, $\geq 100$ m in diameter.	Generally, not associated with small graben. Rarely, diffusive troughs can be associated with features of this class.
Advanced degraded	Features with moderate to gentle slopes and well-rounded edges.	Rarely deform and crosscut craters with diameters of several kilometers.	No small graben associated with those features.
Heavily degraded	Features with gentle slopes and often indistinctive morphologies, not following the standard wrinkle morphology described in Section 2.1.	Generally, do not crosscut superimposed craters.	No small graben associated with those features.

*Note.* Slopes and morphological descriptions are described relative to each other.

## 4. Results

A total of 242 wrinkle ridges, 137 lobate scarps, and 148 unidentified structures, with a total length of  $\sim 10,991$  km, were mapped in this study (Figure 3). The length of individual segments ranges from  $\sim 1$  km to  $\sim 175$  km, with a mean length of  $\sim 21$  km. The mapped wrinkle ridges have a total length of  $\sim 7,852$  km and range from  $\sim 3.7$  to  $\sim 175$  km. The wrinkle ridge mean length is 32.8 km. Lobate scarps have a total length of  $\sim 946.4$  km with a minimum length of  $\sim 1$  km and a maximum length of  $\sim 58.5$  km. The lobate scarp mean length is  $\sim 7$  km.

The differences in the appearance of the ridge segments allow distinguishing four different classes. These classes are crisp, moderately degraded, advanced degraded, and heavily degraded. They differ from one another in their erosional state, general structure, surface texture, crosscut relationships, and small graben occurrence. However, transitions between the different degradation classes are gradual. A total of 846 segments of contractional tectonic features were mapped, of which 658 segments were classified (Figure 4). Their appearances and occurrences are described in the following.

A total of 49 segments with a cumulative length of  $\sim 451$  km and an average length of  $\sim 9.2$  km were classified as crisp (Figure 5). Consequently, they represent 5.1% of the total mapped length. Crisp features consist of wrinkle ridges and lobate scarps. All of them occur scattered within Mare Tranquillitatis and are often close to moderately degraded features (Figure 4). In general, they have a NW–WNW orientation. Crisp features have sharp edges, and steep slopes on a small scale (<100 m; Figure 5). They are generally relatively small structures in terms of length and width and have a winding and lobate appearance. They often braid and cross each other along the strike. The crisp wrinkle ridges often resemble a lobate scarp morphology, with a simple asymmetrical profile and, in some cases, a seemingly missing broad arch. Often smaller surface-breaking tectonic features occur in their vicinity. Crisp features, generally, crosscut small craters (Figure 5c; <50–100 m diameter) and wrinkle ridges often appear to be surface breaking when they crosscut craters. Clusters of small (width <50 m) crisp appearing graben and troughs are present on top of and in the close vicinity of crisp features (Figure 5). Generally, the graben are located at the hanging wall and are oriented perpendicular and parallel to the latter. Small boulder patches are occasionally visible (Figure 5b).

About 100 segments were classified as moderately degraded (Figure 6). They have a total length of  $\sim 780$  km, which makes up 8.9% of the total mapped length. On average, they have a  $\sim 7.8$  km length and generally show a NW orientation. Moderately degraded features are comprised of lobate scarps and wrinkle ridges. The structures are similar in size to the crisp segments, but the edges can be more indistinct than crisp features. In general, they have a winding and lobe-like morphology, and they often braid and cross each other. Only a few small craters superimpose the segments. They typically crosscut several craters along their length, which mostly have diameters of larger than 100 m (Figure 6). Small graben are generally not associated with these structures. They occur throughout Mare Tranquillitatis and can be spatially associated with crisp, advanced, and heavily degraded features.

Advanced degraded features (Figure 7) are the second most common class and dominantly composed of wrinkle ridges. A total of 251 advanced degraded wrinkle ridges with an average length of  $\sim 11$  km have been mapped,

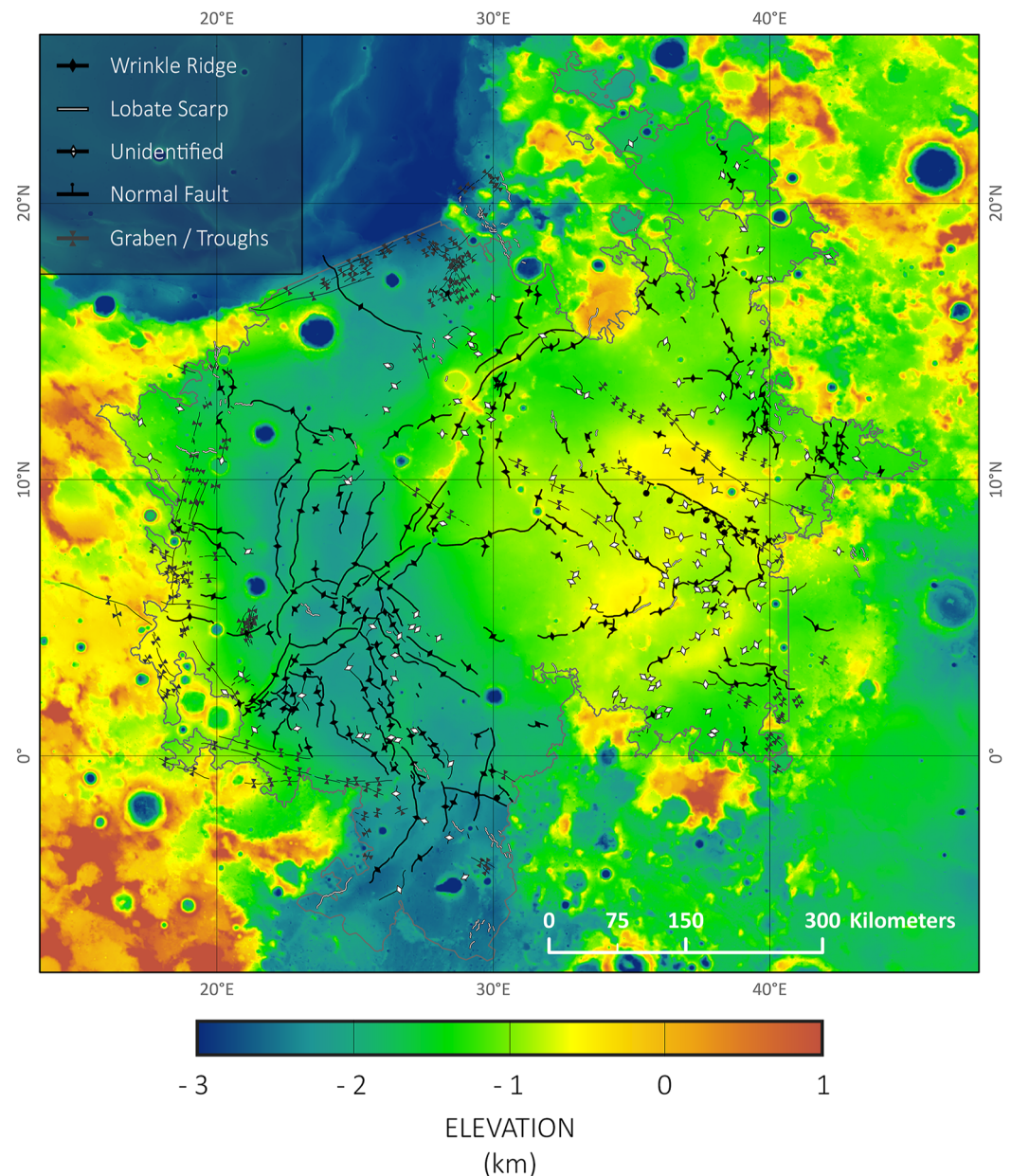


**Figure 3.** The tectonic map of Mare Tranquillitatis projected on the merged LRO LOLA—SELENE Kaguya DEM (Barker et al., 2016). A color-blindness-friendly version can be accessed in the Supporting Information S1 (Figure S1). Parts of the lobate scarp cluster in the northern mare cross the highland boundary and continue into Mare Serenitatis near the Taurus-Littrow valley. Unidentified features are linear positive topographic features with a possible but unproven tectonic origin (other possible origins are, e.g., dikes, lava flows, surface expressions of buried structures, or ejecta remnants).

resulting in a total length of  $\sim 2,762$  km. This class represents 31.5% of the total length. They are generally the most massive wrinkle ridges with respect to width and topography (up to 10 s of kilometers wide and hundreds of meters high). Their rounded morphology mostly resembles the traditional wrinkle ridge definition with a, in some cases km scaled, broad arch and an asymmetric superimposed steep crest (Figure 7a). The changes in the orientation of the wrinkle ridge asymmetry are either gradual or abrupt. Smaller ridge segments of higher order occur in front or back and on the top of these wrinkle ridges. Structures of higher order can transition to first-order ridges along their strike. On slope maps, advanced degraded wrinkle ridges show slopes up to  $>30^\circ$ . They have a larger number of superimposed craters than the previously described morphological classes. However, the abundance of superimposed craters is often lower than crater abundances in the surrounding mare units. These wrinkle ridges



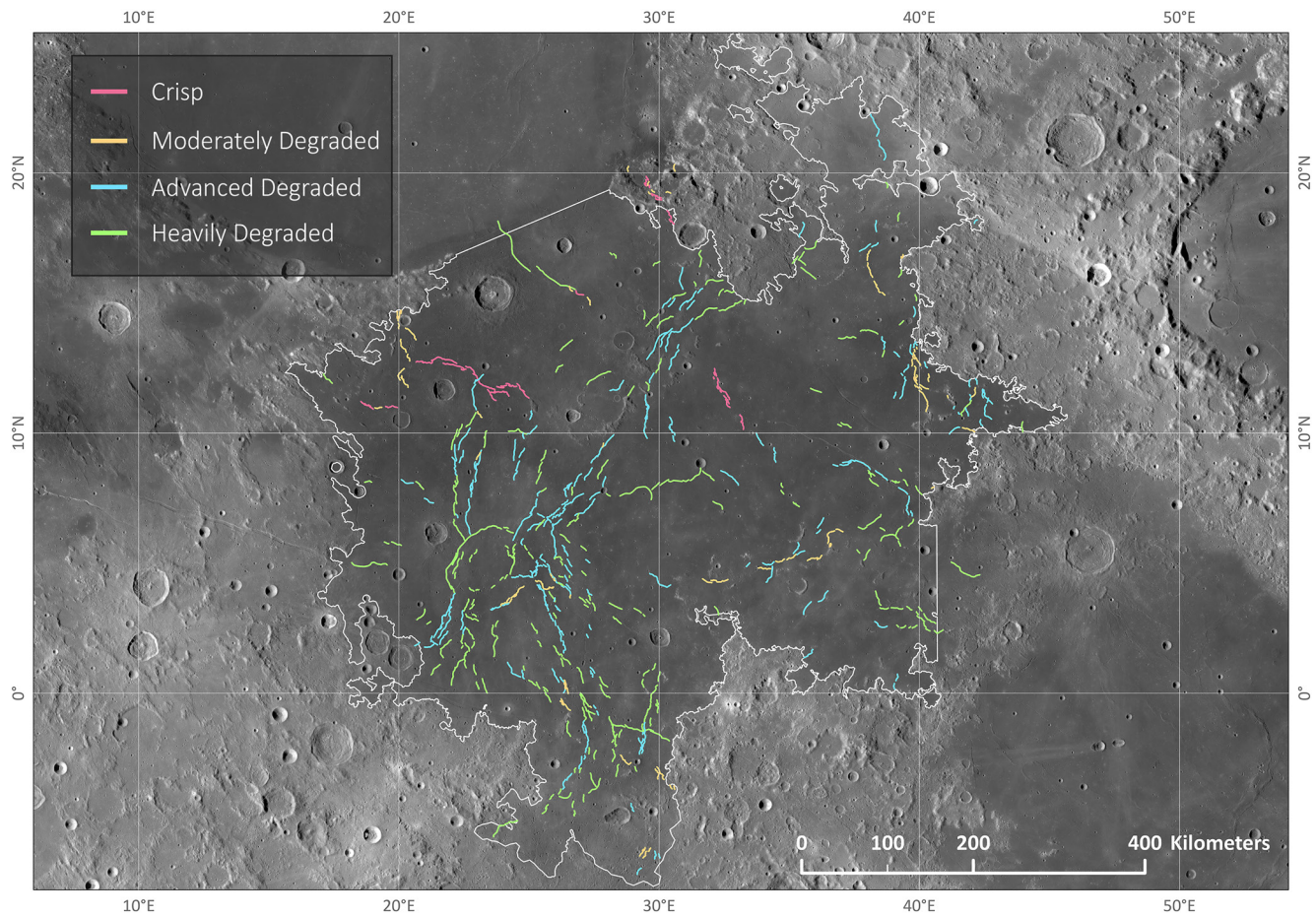


**Figure 4.** Tectonic feature map with all degradational classified segments colorized according to their respective classes and projected onto the WAC global mosaic (Robinson et al., 2012). This map includes wrinkle ridges, lobate scarps, and unidentified features. Tectonic features in the western part mostly composed of advanced and heavily degraded features. Crisp and moderately degraded features occur scattered in clusters throughout the mare.

can deform and crosscut craters with diameters of several hundred meters, but most segments do not crosscut any craters. The surfaces often show a crisscross pattern that previous studies described as an “elephant-hide” pattern (Figure 7b; Bondarenko et al., 2022; Gold, 1972; Zharkova et al., 2020). Extensive boulder fields are associated with some advanced degraded wrinkle ridges (Figure 7).

The most common class are the heavily degraded features (Figure 8), which also dominantly consist of wrinkle ridges. 258 segments, with a total length of ~3,140 km and an average length of ~12.1 km, were mapped. As a result, 35.8% of the total length is represented by this class. While their overall structure can be similar to advanced degraded wrinkle ridges, they generally have an indistinctive and diffuse morphology with more rounded edges (Figure 8), and the classical wrinkle ridge structure is often only visible in topographic data. They have many superimposed craters and generally do not crosscut any craters, but rarely can deform craters with diameters of several hundred meters. There are no associated small graben present. Their surface texture can resemble an elephant-hide structure. In general, advanced and heavily degraded wrinkle ridges are similarly distributed. However, individual wrinkle ridge assemblages are generally represented mainly by one of both classes. In general, heavily degraded wrinkle ridges occur less commonly together with crisp and moderately degraded wrinkle ridges than advanced degraded wrinkle ridges. Both classes represent the largest wrinkle ridge structures in Mare Tranquillitatis in length, width, and height.

## 5. Discussion

The sharp-edged morphology and the relatively small size of the crisp wrinkle ridges and lobate scarps suggest a relatively young formation age in contrast to advanced degraded and heavily degraded features. Crisp features

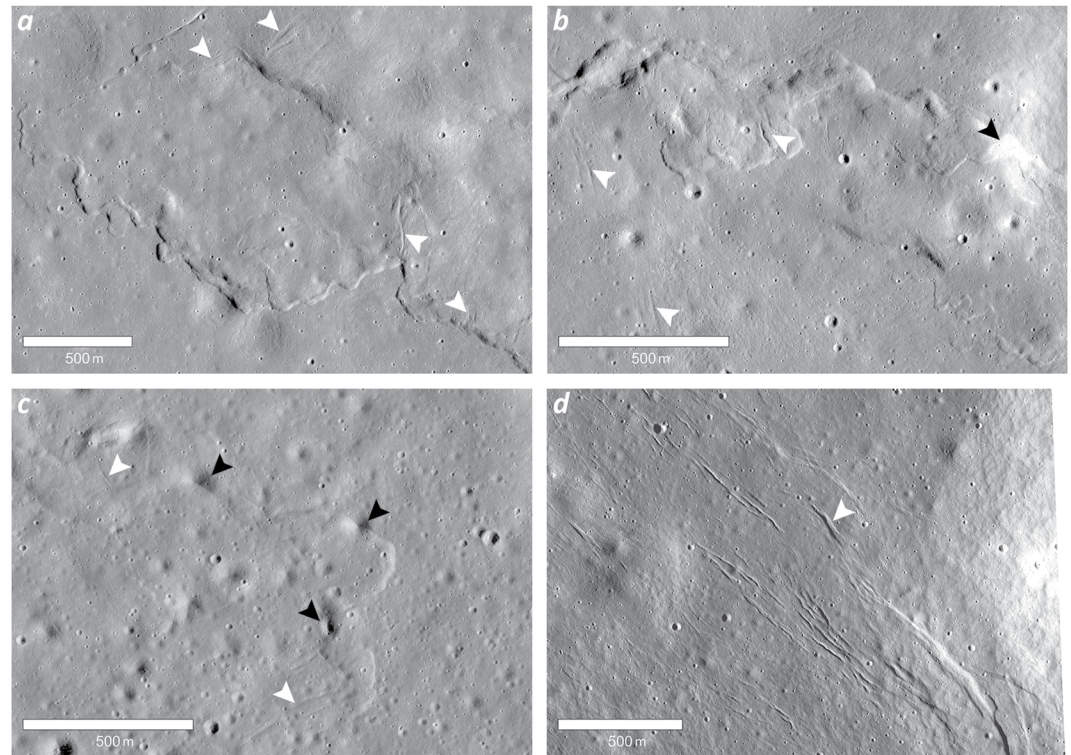


**Figure 5.** Narrow Angle Camera images of crisp features. White arrows show representative graben. (a) Wrinkle ridge north of Ross Crater with a crisp morphology and small graben (M1184668142RE; 11.82°N, 24.27°E). (b) Image of the same wrinkle ridge further west. Visible are several sets of small graben and a small boulder patch (black arrow; M1184668142RE; 11.90°N, 24.17°E). (c) Small and faint lobate scarp in the vicinity of Taurus-Littrow valley. The image shows some faint graben-like features and deformed craters with ~100 to ~50 m in diameter (black arrows; M1154023134RE; 19.11°N, 29.93°E). (d) Set of graben in close vicinity of a crisp lobate scarp cluster near Taurus-Littrow (M1157549836RE; 18.52°N, 30.55°E).

can crosscut craters with diameters of less than 50–100 m. Craters of these sizes are estimated to be of Copernican ages (<800 Ma; Wilhelms et al., 1987), because older craters of this size would have been infilled and degraded since then (Basilevsky, 1976; Fassett & Thomson, 2014; Trask, 1971). Thus, it is possible to establish a Copernican age, that is, an upper age limit of ~800 Ma for these landforms. Since the tectonic activity would result in seismic shaking and thus in enhanced degradation of the small craters, the upper limit is presumably overestimated (Williams et al., 2019). CSFD measurements also support Copernican ages for lobate scarps with similar crisp morphologies (Clark et al., 2017, van der Bogert et al., 2018) and possibly even wrinkle ridges (Valantinas et al., 2018). Accompanying crisp features are small fresh graben and troughs (Figure 5). The existence of small crisp graben situated near lobate scarps was first documented at the back-limb of the Lee-Lincoln scarp, close to the Apollo 17 landing side (Watters et al., 2010). Since then, more of these structures have been found in the vicinity of lobate scarps (French et al., 2015; Watters et al., 2012) and wrinkle ridges (French et al., 2015; Williams et al., 2019). Small graben observed in Mare Tranquillitatis are similar in their dimensions to the graben described in the latter studies. They typically have widths of less than 50 m and, in many cases, of even less than 10 m. Because of their similarity to sizes measured in other studies, depths of ~17–~1 m can be assumed (Watters et al., 2012; Williams et al., 2019). Fill rates of shallow depressions in lunar regolith are estimated to be  $5 \pm 3$  cm/Ma (Arvidson et al., 1975). Therefore, a ~1 m deep graben should be filled entirely with regolith after ~12.5–~50 million years, which implies formation ages of less than 50 Ma. Due to their association with lobate scarps, Watters et al. (2012) suggested that these graben form by uplift and flexural bending resulting from the movement at the underlying thrust fault. Thus, these graben can be viewed as possible evidence for the tectonic activity of crisp features during the last 50 Ma (French et al., 2015; Watters et al., 2012; Williams et al., 2019). Lu et al. (2019), used ejecta boulders of craters crosscut by small wrinkle ridges in Mare Imbrium to calculate the individual crater ages since boulder abundances decrease with exposure time (Basilevsky et al., 2013; Ghent et al., 2014; Lu et al., 2019). The derived ages support wrinkle ridge formation during the last 10 s of Ma (Lu

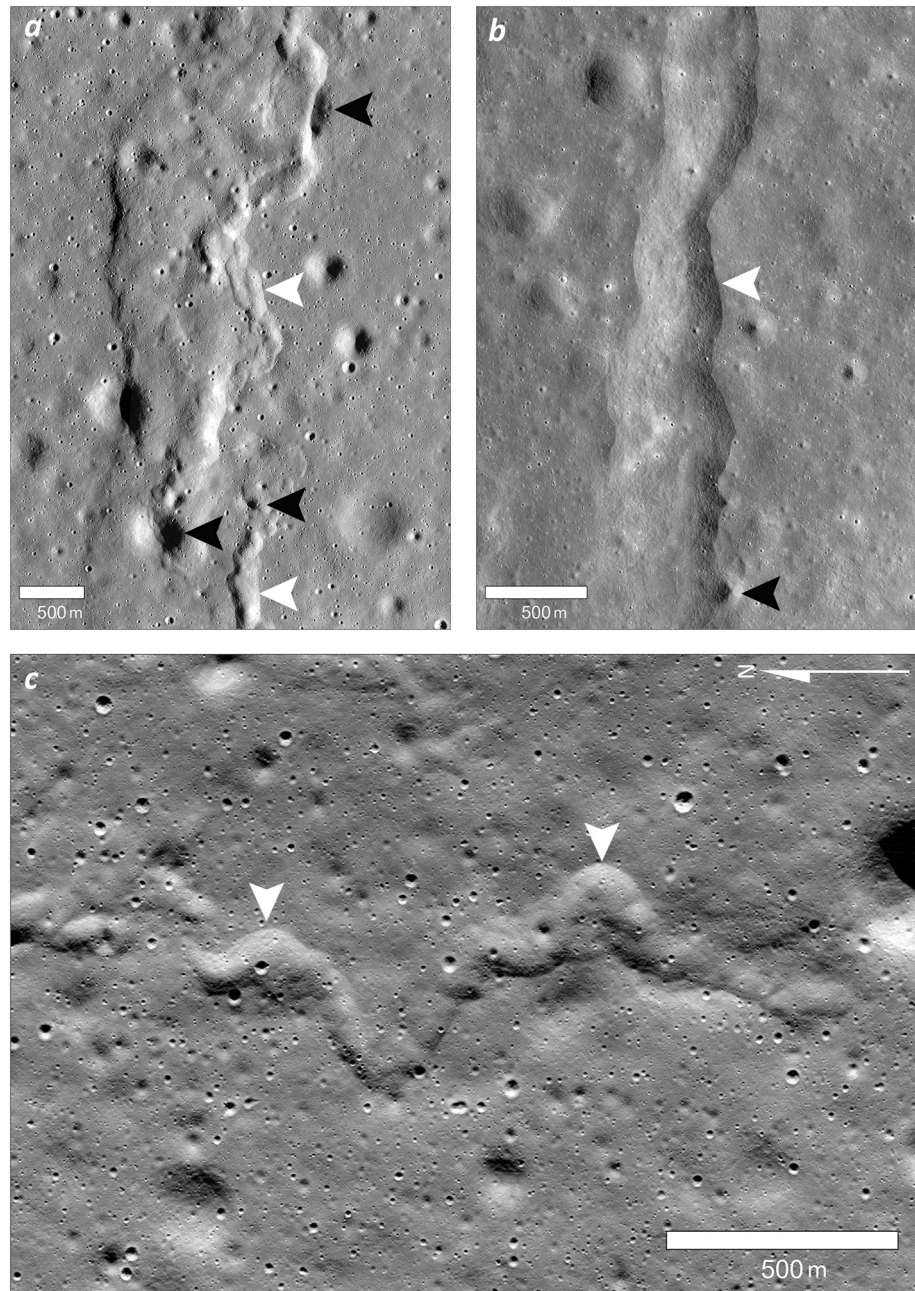


**Figure 6.** Narrow Angle Camera images of moderately degraded features with relatively sharp contacts (white arrows) in Mare Tranquillitatis. (a) A moderately degraded wrinkle ridge in the eastern mare deforming and cross-cutting several craters (black arrows; M1245756057LE/RE; 12.29°N, 39.82°E) and (b) a small moderately degraded lobate scarp in the northwestern mare which also deforms a ~100 m diameter crater (black arrows; M1279976340LE; 14.60°N, 20.04°E).

et al., 2019). The morphology of the young wrinkle ridges studied by Lu et al. (2019) are indistinguishable from crisp wrinkle ridges in Mare Tranquillitatis. In summary, different methods indicate the formation of young wrinkle ridges and lobate scarps on the Moon during the last few 10 to 100 Ma. Thus, we propose tectonic activity for crisp wrinkle ridges and lobate scarps in Mare Tranquillitatis at least during the last 50 Ma, which further highlights the recent tectonic activity of the Moon.

Based on our study, we cannot conclusively estimate formation ages for moderately degraded features. Crater crosscutting relationships imply younger ages for moderately degraded wrinkle ridges and lobate scarps than advanced degraded features. The main difference between moderately degraded and crisp features, next to a more

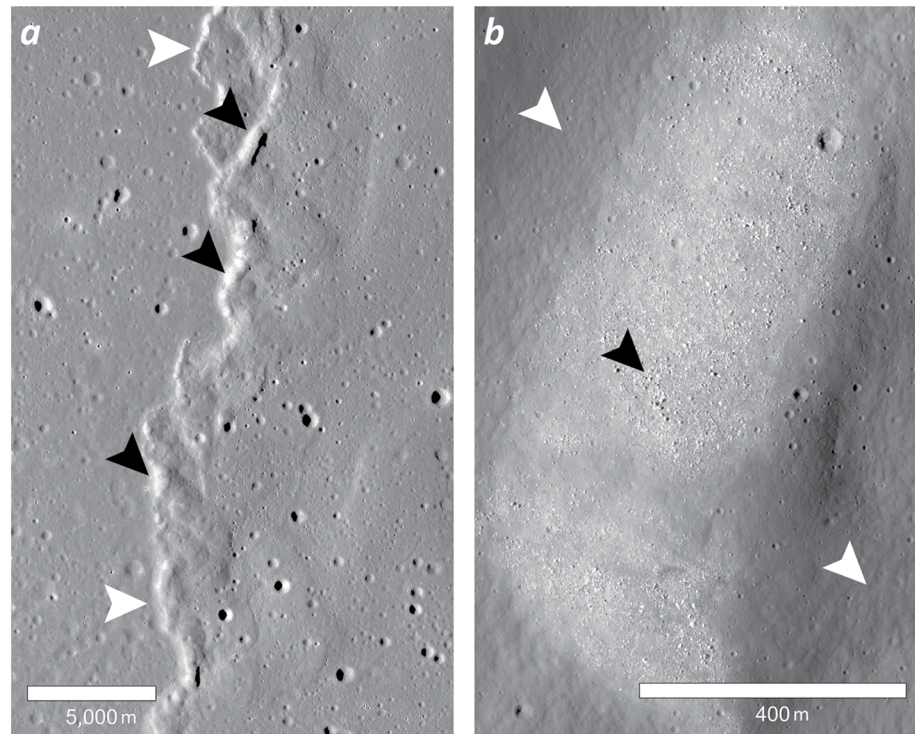


**Figure 7.** Kaguya Terrain Camera images of representative advanced degraded wrinkle ridges. The advanced degraded wrinkle ridge (7.54°N, 22.75°E) has a well-developed wrinkle ridge morphology consisting of a broad arch and a superimposed ridge (white arrows). In addition, it exhibits several dominant boulder fields, which are visible as bright spots along the ridge (black arrows). (b) Close up Narrow Angle Camera image (M1234102538LE) of the ridge shown in (a), featuring boulder fields (black arrow) and the “elephant-hide” texture (white arrows).

rounded morphology, is the apparent lack of small graben. However, while small graben can be seen as possible evidence for recent tectonic activity, it is unknown whether they necessarily have to form during the recent activity. Therefore, the lack of crisp graben does not necessarily imply an older age. Furthermore, because of the small size and faint appearance of these graben, as well as the missing NAC coverage (incidence angles between 55° and 90°) of some features, a wider distribution of undetected graben is possible. We estimate that moderately degraded wrinkle ridges and lobate scarps have a broad range of formation ages in between crisp and advanced degraded features.

Crisp features occur scattered within Mare Tranquillitatis and do not align with patterns predicted by basin loading and subsidence. Hence, subsidence does not seem to be the major controlling factor of young wrinkle ridge and lobate scarp formation. Additionally, they are not correlated with positive gravitational anomalies within the mare (Figures 9 and 10). However, as previously stated, Mare Tranquillitatis is of irregular shape, which could influence subsidence-induced stress patterns, and the role of the thickness of the elastic lithosphere in the wrinkle ridge formation is also a factor (Watters, 2022). Previous studies have discussed the prolonged cooling, triggered by the abundance of heat-producing elements, of the Procellarum KREEP Terrane (PKT) to be a factor in the recent wrinkle ridge formation (Daket et al., 2016; Lu et al., 2019). However, Mare Tranquillitatis is not associated with the PKT (Wieczorek & Phillips, 2000). Therefore, this model does also not explain the recent formation of wrinkle ridges and lobate scarps in Mare Tranquillitatis. Late-stage global compressional stresses are consistent with both an initially completely molten Moon and an initially hot exterior and magma ocean (Binder & Gunga, 1985; Solomon & Head, 1979; Watters et al., 2019; Williams et al., 2013). The interior cooling of the Moon could result in compressional stresses of  $\geq 2$ , but  $< 10$  MPa (Watters et al., 2015, 2019). For shallow thrust faults to form, an estimated  $\sim 2$ – $7$  MPa is sufficient (Watters et al., 2019; Williams et al., 2013). Small-scale wrinkle ridges were likely formed by shallow thrust faults (Lu et al., 2019; Watters, 2004). The derived depths from Lu et al. (2019) for small wrinkle ridge thrust faults are similar to those suggested depths of shallow lobate scarps ( $\sim 1$  km; Williams et al., 2013). Concluding, global compression seems to be a likely

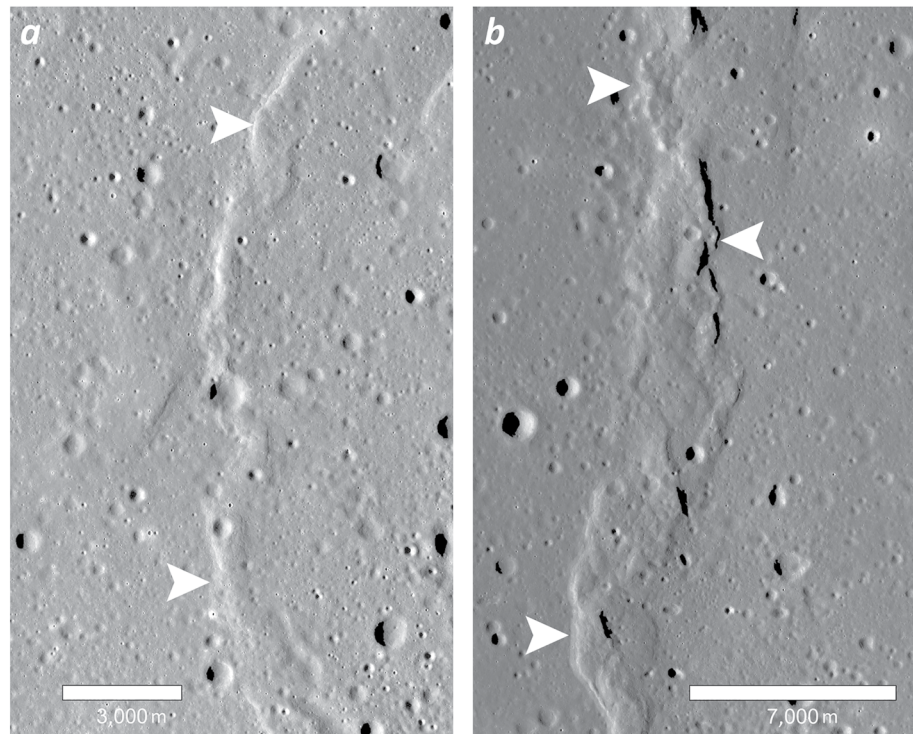


**Figure 8.** Kaguya Terrain Camera images of representative heavily degraded wrinkle ridges (white arrows). Both wrinkle ridges (a), 1.31°N, 22.56°E; (b), 8.10°N, 22.20°E) have gentle slopes and less well-developed wrinkle ridge morphologies than those seen in Figure 7. The ~1 km-sized crater in the center of image (a) resembles a rare case, which shows the possible deformation of a crater by a heavily degraded ridge. Survival times of ~1 km-sized craters are still estimated to be several billion years (Fassett & Thomson, 2014).

candidate as the driving force behind the recent wrinkle ridge and lobate scarp formation on the Moon and in Mare Tranquillitatis. Global lobate scarp patterns and the timing of detected moonquakes highlighted the possible influence of tidal forces, such as orbital recession, diurnal tidal stresses, and true polar wander onto the lunar stress field (Matsuyama et al., 2021; Watters et al., 2019). Models of an additional influence of SPA ejecta loading onto the global stress field also showed good fitting results and are discussed as an alternative or addition to the influence of tidal forces (Matsuyama et al., 2021). N to NW orientated faults between ~20°E and ~40°E, and ~0°N to ~20°N are predicted by a combination of recession stresses, diurnal tidal stresses at apogee, and global contraction (Watters et al., 2015, 2019), as well as by a combination of SPA loading, true polar wander, and global contraction (Matsuyama et al., 2021). These predicted trends approximately correspond to the W to NW orientation of crisp ridges and scarps within Mare Tranquillitatis (Figure 11), suggesting their formation is consistent with those models. However, it should be highlighted that the lithospheric stress field is a result of complex interaction and overlaying of multiple stresses, evolving with time. Additional influences like, for example, late stage mare basalt cooling (Tian et al., 2021), stresses related to a possible movement of magma in connection with the young volcanic activity in Mare Tranquillitatis (Braden et al., 2014; Qiao et al., 2020), or preexisting ancient faults in the basement might have influenced the regional stress field. The patterns of moderately degraded wrinkle ridges align with both the patterns of advanced and heavily degraded features, as well as with some crisp ridges and scarps (Figure 4). Hence, moderately degraded wrinkle ridges and scarps could reflect the evolution of the stress field from dominantly basin-localized to a dominantly global stress field, and they could represent the continued growth of older faults.

The large size and strongly degraded morphology of advanced and heavily degraded features suggest an older formation age relative to moderately degraded and crisp features. Advanced and heavily degraded features deform all the mare units defined by Hiesinger et al. (2000), which have ages of ~3.4–~3.8 Ga. Consequently, they have an upper formation age limit of at least 3.8 Ga. Since Rupes Cauchy and some large graben are deformed by advanced and heavily degraded wrinkle ridges, some of the wrinkle ridge formation occurred after 3.6 Ga

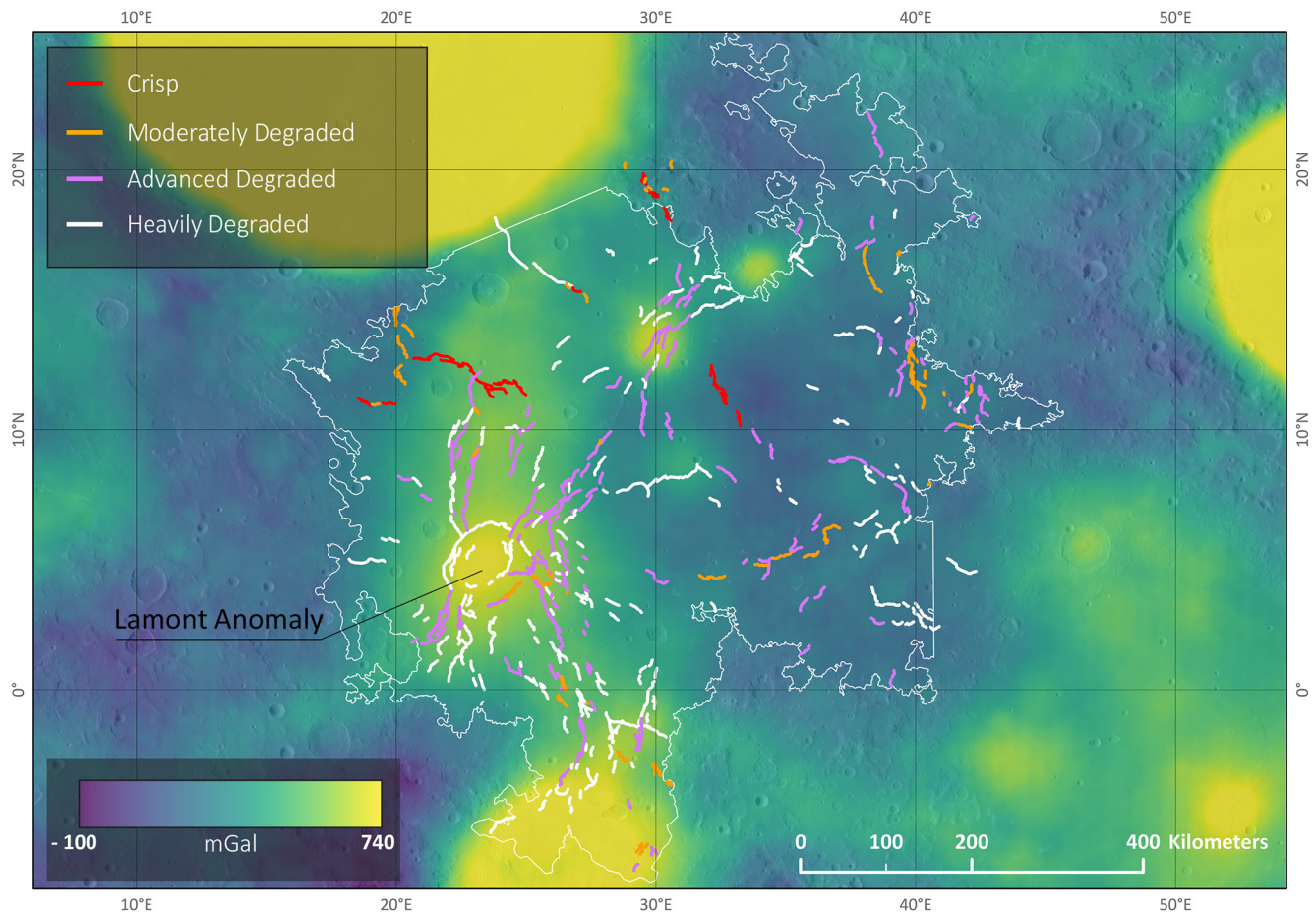


**Figure 9.** Bouguer anomaly map of Tranquillitatis superposed on the WAC global mosaic. The map has the same spatial extent as the map in Figure 4, and shows the tectonic feature map of Figure 4. The outline of Mare Tranquillitatis is shown as a fine white line. Yellowish colors indicate positive gravitational anomalies, which implies a thin crust and mantle upwelling, as well as thick abundance of basalt. Mascon basins like Mare Serenitatis in the northwestern part of the map are represented in yellow colors, whereas non-mascon basins like Mare Tranquillitatis appear in more heterogenous and mainly in blue and green colors. The western part of Mare Tranquillitatis has more pronounced positive gravitational anomalies than the eastern part. Concentric wrinkle ridges occur at the positive Lamont anomaly in southwestern Tranquillitatis. Crisp and moderately degraded features are not correlated with gravitational anomalies.

(Lucchitta & Watkins, 1978; Watters & Johnson, 2009). They can deform craters of several hundred meters in diameter but generally deform no craters, which agrees with Nectarian, Eratosthenian, and Imbrian formation ages (Trask, 1971). The deformation of craters with diameter ranges of hundreds of meters implies on the basis of crater degradation (Basilevsky, 1976; Fassett & Thomson, 2014) that at least some wrinkle ridges experienced ongoing activity throughout the Nectarian, Eratosthenian, and possibly even the Copernican. Yue et al. (2017) found a young average age of large wrinkle ridges in Mare Tranquillitatis ( $\sim 2.4$  Ga) relative to other Maria ( $\sim 3.3$  Ga). With the focus on Mare Tranquillitatis and the degradation-state approach of our classification, this age discrepancy between wrinkle ridges in Mare Tranquillitatis and other Maria cannot be resolved. Relatively younger ages of advanced degraded wrinkle ridges compared with heavily degraded ridges can only be suggested and not conclusively proven. More precise dating methods than our morphological analysis are needed to uncover the early tectonic evolution of the Maria basins; however, standard CSFD measurements on wrinkle ridges are challenging, because of steep slopes, small count areas, and the often hummocky and heterogeneous terrain (Frueh et al., 2020). Hence, buffered crater counting might be a more suitable option to obtain the formation ages of individual wrinkle ridges.

The occurrence of the advanced and heavily degraded concentric and radial wrinkle ridges in the western mare appears to have been localized by a subsurface feature (Figures 9 and 10; Freed et al., 2001; Schleicher et al., 2019). These concentric and radial wrinkle ridges, as well as several concentric large graben, can be attributed to the Lamont gravity anomaly, which is argued to be a ghost crater (Dvorak & Phillips, 1979; Scott, 1974)

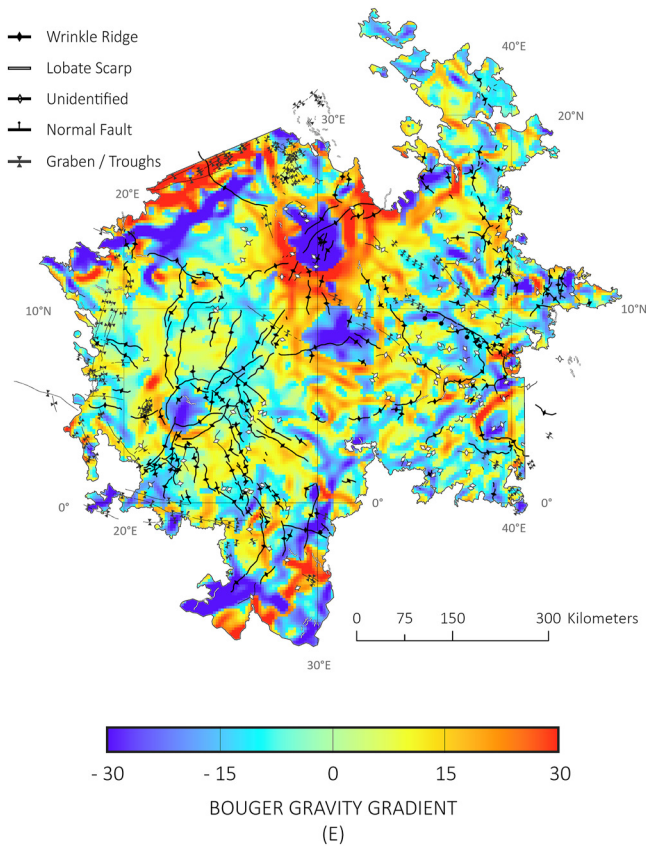


**Figure 10.** Grail bouguer gravity gradients map of Mare Tranquillitatis (Supporting Information from Andrews-Hanna et al., 2018) in units of Eötvös ( $1 \text{ E} = 10^{-9} \text{ s}^{-2}$ ) and our tectonic map of Figure 3. Gravity gradient maps are used to identify buried deep-seated structures, such as large igneous intrusions and ring-faults in impact basins (e.g., Andrews-Hanna et al., 2013, 2014, 2018; Valantinas & Schultz, 2020). Eastern Tranquillitatis does not exhibit clearly detectable anomalies known from deep faults.

or a feature of volcanic origin (Zhang et al., 2018). Next to the Lamont anomaly, western Mare Tranquillitatis is characterized by a positive gravitational anomaly ranging from Mare Nectaris in the south to Mare Serenitatis in the north (Figures 9 and 10). Correlated with this positive anomaly are the thickest basalts in Mare Tranquillitatis (De Hon, 1974, 2017; Dvorak & Phillips, 1979; Konopliv et al., 2001; Zuber et al., 2013). At the surface, this positive anomaly is expressed as an elongated depression. Advanced and heavily degraded wrinkle ridges and large graben within this depression occur parallel to the gravitational anomaly and the topographic depression, which could also imply a subsidence-related origin (Figures 3 and 9; McGovern et al., 2022). Mare Serenitatis most likely influenced the north-western Mare Tranquillitatis, resulting in a radial wrinkle ridge and parallel graben to Mare Serenitatis (Figure 3). Wrinkle ridges close to the eastern mare boundary follow a NS trend similar to the general trend of the eastern boundary itself, which is consistent with an origin from basin loading and subsidence. The eastern mare boundary shows no clearly detectable gravitational anomalies that have been associated with deep fractures of the mare basement (Figure 10; Andrews-Hanna et al., 2018). The fewer number and the less coherent patterns of features in the eastern mare could be a result of the shallower basalts and, therefore, less basin loading induced by subsidence. While basin loading and subsidence influenced the regional stress field and the tectonic patterns in Tranquillitatis, additional global stress fields contributing to wrinkle ridge formation have been proposed. One possible influence on the global stress field is deep transient stresses generated by the SPA basin (Schultz & Crawford, 2011), which predicts antipodal failures on the lunar nearside due to extensions deep within the Moon. Schultz and Crawford (2011) suggested that reactivated deep-seated faults localized the wrinkle ridges. Wrinkle ridge patterns of the lunar nearside do spatially correlate with the predicted patterns (Schultz & Crawford, 2011; Valantinas & Schultz, 2020); however, it is not clear that SPA-related stresses would not have largely relaxed before the period of wrinkle ridge formation in Tranquillitatis. Another discussed potential model is the fault adjustment correlated with deep-seated intrusions on the lunar nearside. In this case, wrinkle ridges would be the surface expression of these deep-seated intrusions (Andrews-Hanna et al., 2014). GRAIL Bouguer gravity gradient data

revealed a possible polygonal pattern of ancient deep intrusion connecting most of the lunar Maria and also Mare Tranquillitatis (Andrews-Hanna et al., 2014). The western elongated positive gravitational anomaly of Mare Tranquillitatis is proposed to originate from these deep-seated intrusions. However, following the linear unrestricted growth trends and the similar displacement values of wrinkle ridges associated and not associated with these proposed intrusions, there is little evidence that most of the ridge faults were influenced by buried structures associated with ancient rifts (Watters, 2022). Having said that, we do observe wrinkle ridges correlated with sharp increases in elevation, possible extensive folding, and an elevation offset between both sites of the fold located in this western part of the basin. Possible similar wrinkle ridges have been associated with deeply rooted faults penetrating the base of mare deposits (Byrne et al., 2015; Watters, 2022). The slopes of the trough associated with the positive gravitational anomaly, however, complicate the assessment of the actual extent of folding. Quantifying the deformation in Mare Tranquillitatis will be part of a planned follow-up study. In summary, the compressional stresses that resulted in the formation of advanced and heavily degraded wrinkle ridges in Mare Tranquillitatis originated primarily from load-induced subsidence with other possible sources of regional or global stress, like SPA-induced stress and fault adjustment, which changed with time. Individual wrinkle ridges in western Tranquillitatis could be correlated with deep-rooted faults.

It should be noted that the ancient age of advanced and heavily degraded feature, which we imply in this study, is the formation age and not necessarily the age of the most recent activity along the fault. Previous studies have discussed the possible activity of ancient wrinkle ridges during the last Ma (French et al., 2019; Valantinas & Schultz, 2020). One possible evidence is the abundance of boulders at wrinkle ridge crests (French et al., 2019;

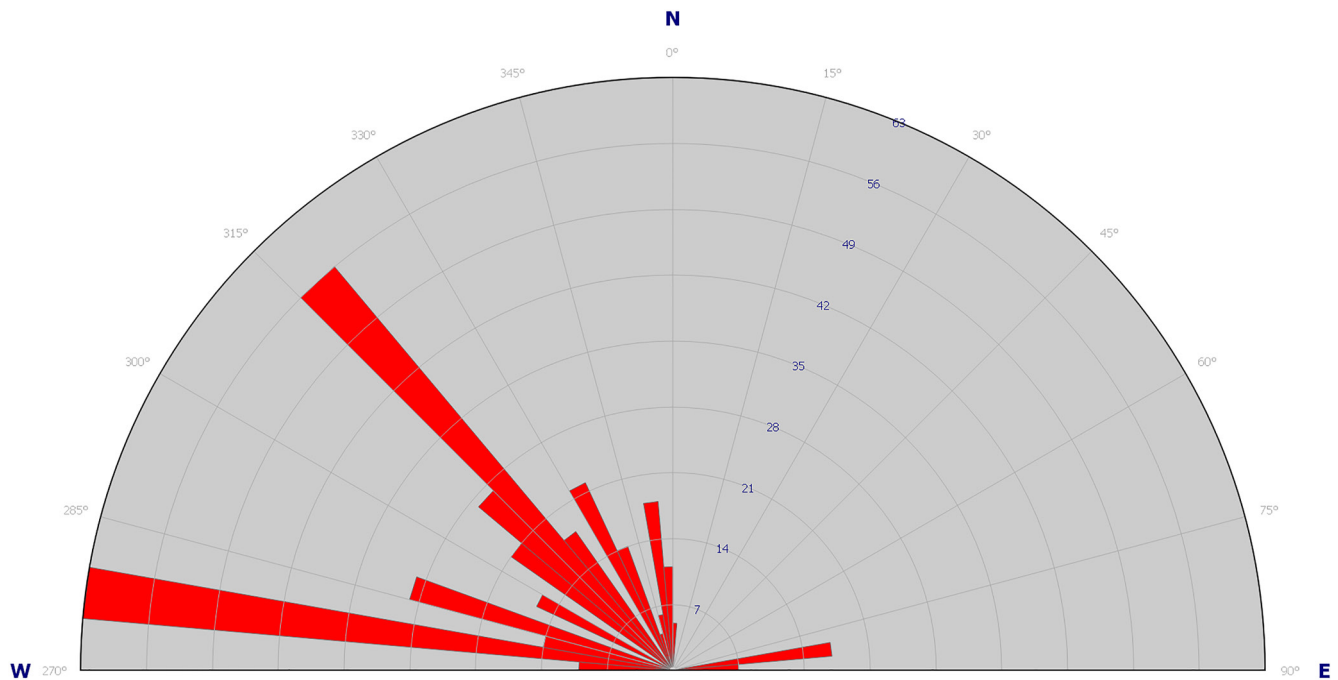


**Figure 11.** Rose diagram of the orientations of crisp features within Mare Tranquillitatis, including lobate scarps and wrinkle ridges. Crisp features share a western to northwestern orientation.

Valantinas & Schultz, 2020; Valantinas et al., 2017; Watters et al., 2019). Valantinas and Schultz (2020) suggested that layered mare basalts buckled and regolith drained into small fractures during episodes of uplift, exposing the buckled material below. Basilevsky et al. (2013) and Ghent et al. (2014) found that 50% of rock populations, with fragment diameters larger than 2 m, are destroyed after 40–80 Ma and 99% after 150–300 Ma. Following the boulder size of wrinkle ridge boulder fields, Valantinas and Schultz (2020) proposed that wrinkle ridges with high boulder abundance were active during the last tens of millions of years. Boulder density increases with increasing slope. This leads to the question whether boulders are simply associated with steep slopes rather than ongoing wrinkle ridge activity since shallow seismic shaking generated by impacts or tectonic activity unrelated to wrinkle ridges could also result in the exposure of boulder fields (French et al., 2019). For our classification, the abundance of boulders was not used to determine the possible erosional state of a wrinkle ridge segment. Crisp and moderately degraded features usually do not appear in DiVINER rock abundance maps and boulders are only occasionally visible in small patches. Thus, no or merely a few boulders have been exposed during their activity. This could be either evidence against boulder fields as a general sign of recent tectonic activity, related to the relation between flow thickness and thrust fault size, or correlated with the physical properties of the basalt flows, which result in different predicted rock abundances (Elder et al., 2022). Boulder-rich wrinkle ridges mapped by Valantinas and Schultz (2020) tend to correlate with advanced degraded wrinkle ridges rather than heavily degraded. However, it should be noted that the boulder fields themselves could influence the morphological classification since they typically appear brighter than the regolith (Figure 7a), possibly resulting in a greater contrast between the sunlit and shadow sides and, therefore, in a seemingly more defined appearance. Five segments from Valantinas and Schultz (2020) can be associated with moderately degraded wrinkle ridges. These are located at the southeastern Lamont ring and a single wrinkle ridge in the southwestern Mare Tranquillitatis (Figure 12). All of these ridges occur together with advanced and heavily degraded wrinkle ridges and are larger in relief than other moderately degraded features. They deform craters with ~100 m in diameter or are accompanied by faint and small graben-like features (Figure 12b). The size of those moderately degraded wrinkle ridges, their transitional morphology between moderately degraded and advanced degraded features, and their associated patterns with advanced and heavily degraded wrinkle ridges suggest possible ancient wrinkle ridges, which were later modified by more recent activity. Two large wrinkle ridges directly north of the Lamont Anomaly could also contribute to this discussion (Figures 3, 4, and 9). The eastern ridge (7.0°N, 22.7°E) shows a high boulder abundance, while the western ridge (7.0°N, 22.1°E) only exhibits boulder



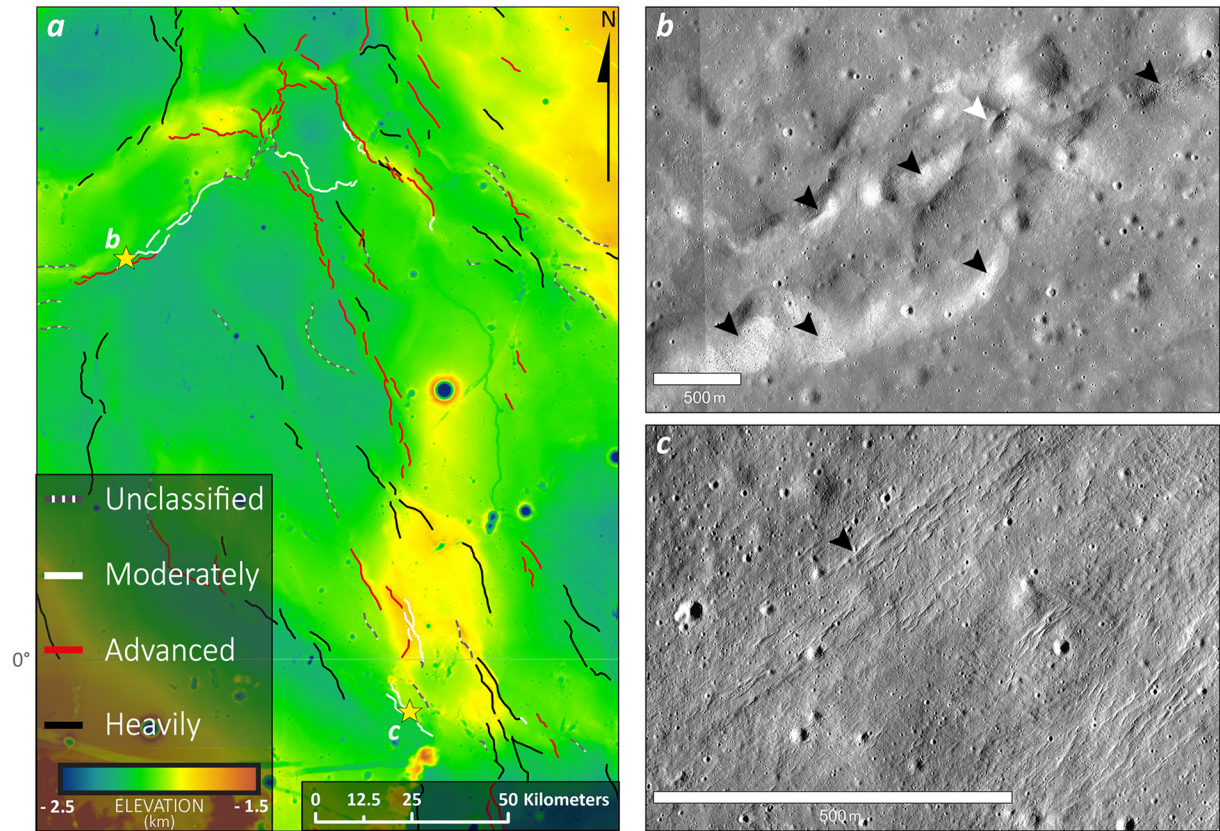


**Figure 12.** Evidence for recent activity by ancient wrinkle ridges in Mare Tranquillitatis. (a) Shows the topographic map of the region southeast of the Lamont anomaly. The stars mark the locations of (b, c). (b) Shows NAC image (M1108125194LE; 3.43°N, 23.97°E) showing a part of a concentric wrinkle ridge at the southeastern Lamont anomaly. It crosscuts craters with ~100 m in diameter (white arrow) and exhibits several boulder fields (black arrows). (c) NAC image (M162134363LE) of faint graben-like features on the hanging wall of a wrinkle ridge (0.45°S, 26.47°E). A color-blindness-friendly version can be accessed in the Supporting Information S1 (Figure S2).

fields in its northern most part (Valantinas & Schultz, 2020). Segments of the eastern ridge are classified as advanced degraded and segments of the western ridge, mainly, as heavily degraded. Additionally, the eastern wrinkle ridge shows one small off-shoot segment, which is classified as moderately degraded (Figure 4). The off-shoot segment could highlight the continuing growth of the eastern wrinkle ridge, which resulted in the formation of boulder fields. In those cases, boulder fields might be a sign of recent activity of the wrinkle ridges. However, since boulders might also be exposed due to seismic shaking unrelated to wrinkle ridges (French et al., 2019) and boulder fields can also be found on other positive relief features than wrinkle ridges, we are not able to conclude if all boulder-rich wrinkle ridges in Mare Tranquillitatis are boulder-enriched due to their recent tectonic activity. In addition, crisp and moderately degraded features have not exposed extensive boulder fields. Thus, we can neither clearly support nor reject boulder fields along wrinkle ridges as a general sign of recent tectonism.

Boulder-rich wrinkle ridges on the lunar nearside are proposed to be part of an ANTS. A possible origin of this recent activity was assigned to the previously discussed deep transient stresses generated by the SPA basin (Schultz & Crawford, 2011; Valantinas & Schultz, 2020) and a continued fault adjustment correlated with deep-seated intrusions (Andrews-Hanna et al., 2014; Valantinas & Schultz, 2020). Recorded deep moonquakes might be evidence of the SPA-induced stresses (Valantinas & Schultz, 2020). However, as previously stated, the influence of these proposed putative mare-filled ancient rifts and intrusions on wrinkle ridge formation has been questioned (Watters, 2022). Also, it remains unknown if the current lunar stress field would allow for ongoing readjustment of those ancient faults. Thus, the question of young activity associated with ancient wrinkle ridges and the implications of boulder fields remains unresolved. The reactivity or prolonged activity of ancient wrinkle ridges, however, seems to be true for at least some individual wrinkle ridges in Mare Tranquillitatis.

## 6. Conclusions

In this study, compressional tectonic features were mapped in Mare Tranquillitatis and classified into crisp, moderately degraded, advanced degraded, and heavily degraded, based on their morphology and erosional state. This classification allows us to suggest formation ages and possible origins of these features:

- Crisp features show various signs of recent activity and presumably have an age of tens of Ma (~50 Ma). Based on recent studies and the shared orientation of crisp features, they likely formed due to a combination of global contraction and an additional influence of tidal forces and/or SPA ejecta loading.
- Moderately degraded features, presumably, have a broad range of formation ages in between crisp and advanced degraded features. They could reflect the evolution of the stress field from dominantly basin-localized to a dominantly global stress field, and they represent the continued growth of ancient faults.
- Advanced and heavily degraded features presumably formed in the early history of Mare Tranquillitatis, starting at ~3.8 Ga. The distributions and orientations of those wrinkle ridges indicate complex tectonic patterns and combined stresses. Ancient ridges in western Mare Tranquillitatis have concentric, partly radial, and linear wrinkle ridge patterns associated with basin loading and subsidence. There are scarce signs of the recent activity of some individual ancient wrinkle ridges within the last 100 Ma.

Mare Tranquillitatis exhibits compressional tectonic features with a variety of formation ages ranging from ancient to recent. The complex and changing stress field behind the wrinkle ridge formation is presumably a result of a combination of different factors, which underlines the need for new studies. Furthermore, our results highlight and strengthen the case for a still tectonically active Moon within and outside of the Maria basins. To further uncover the active lunar tectonism, the future installation of a geophysical network on the Moon is highly desirable (Fuqua Haviland et al., 2022).

## Data Availability Statement

Our shapefiles of the tectonic and compressional feature maps are available on Zenodo (Frueh et al., 2023). Kaguya TC images can be obtained from the SELENE Data Archive (<https://darts.isas.jaxa.jp/planet/pdap/selene/>). The TC morning and evening image files can be downloaded from the *sln-1-tc-4-evening-map-v4.0/* and *sln-1-tc-4-morning-map-v4.0/* folders in the directory. LROC image data (Robinson, 2009) are available from the Lunar Orbital Data Explorer, which is produced by the NASA Planetary Data System Geosciences Node. The SLDEM2015 global map (Barker et al., 2016) is available on the Planetary Data System (Neumann, 2009) and at <http://imbrium.mit.edu/DATA/SLDEM2015/>. Global GRAIL gravity anomaly maps are available in the rsdmap directory of Kahan (2013). The GRAIL Bouguer gravity gradient map was accessed from the Supporting Information S1 from Andrews-Hanna et al. (2018). Additionally, LRO, Kaguya, and GRAIL data can be accessed with Quickmap (<https://quickmap.lroc.asu.edu>). The shown rose diagram was created with GeoRose 0.5.1 (Yong Technology Inc, 2014).

## Acknowledgments

The authors thank the LROC teams and LRO engineers for obtaining the essential data. We also thank the SELENE (KAGUYA) TC team and the SELENE Data Archive for providing the SELENE (KAGUYA) data. We acknowledge the use of imagery from Lunar QuickMap (<https://quickmap.lroc.asu.edu>), a collaboration between NASA, Arizona State University & Applied Coherent Technology Corp. Lastly, we wish to thank our reviewers, who provided thoughtful and thorough comments, improving our publication significantly. Open Access funding enabled and organized by Projekt DEAL.

## References

- Andrews-Hanna, J. C., Asmar, S. W., Head, J. W., Kiefer, W. S., Konopliv, A. S., Lemoine, F. G., et al. (2013). Ancient igneous intrusions and early expansion of the Moon revealed by GRAIL gravity gradiometry. *Science*, 339(6120), 675–678. <https://doi.org/10.1126/science.1231753>
- Andrews-Hanna, J. C., Besserer, J., Head, J. W., Howett, C. J. A., Kiefer, W. S., Lucey, P. J., et al. (2014). Structure and evolution of the lunar Procellarum region as revealed by GRAIL gravity data. *Nature*, 514(7520), 68–71. <https://doi.org/10.1038/nature13697>
- Andrews-Hanna, J. C., Head, J. W., Johnson, B. C., Keane, J. T., Kiefer, W. S., McGovern, P. J., et al. (2018). Ring faults and ring dikes around the Orientale basin on the Moon. *Icarus*, 310, 1–20. <https://doi.org/10.1016/j.icarus.2017.12.012>
- Arvidson, R., Drozd, R. J., Hohenberg, C. M., Morgan, C. J., & Poupeau, G. (1975). Horizontal transport of the regolith, modification of features, and erosion rates on the lunar surface. *The Moon*, 13(1–3), 67–79. <https://doi.org/10.1007/BF00567508>
- Barker, M. K., Mazarico, E., Neumann, G. A., Zuber, M. T., Haruyama, J., & Smith, D. E. (2016). A new lunar digital elevation model from the lunar orbiter laser altimeter and SELENE terrain camera. *Icarus*, 273, 346–355. <https://doi.org/10.1016/j.icarus.2015.07.039>
- Basilevsky, A. T. (1976). On the evolution rate of small lunar craters. *Proceeding Lunar Science Conference*, 7, 1005–1020.
- Basilevsky, A. T., Head, J. W., & Horz, F. (2013). Survival times of meter-sized boulders on the surface of the Moon. *Planetary and Space Science*, 89, 118–126. <https://doi.org/10.1016/j.pss.2013.07.011>
- Bhatt, H., Chauhan, P., & Solanki, P. (2020). Compositional mapping and the evolutionary history of Mare Tranquillitatis. *Journal of Earth System Science*, 129(1), 45. <https://doi.org/10.1007/s12040-019-1302-7>
- Bickel, V. T., Aaron, J., Manconi, A., & Loew, S. (2021). Global drivers and transport mechanisms of lunar rockfalls. *Journal of Geophysical Research: Planets*, 126(10), e2021JE006824. <https://doi.org/10.1029/2021JE006824>
- Binder, A. B., & Gunga, H. C. (1985). Young thrust-fault scarps in the highlands: Evidence for an initially totally molten Moon. *Icarus*, 63(3), 421–441. [https://doi.org/10.1016/0019-1035\(85\)90055-7](https://doi.org/10.1016/0019-1035(85)90055-7)

- Bondarenko, N. V., Kreslavsky, M. A., Zubarev, A., & Nadezhkina, I. (2022). "Elephant hide" texture on the moon: Preliminary results on topographic properties. In *53rd lunar and planetary science conference*. Abstract #2469.
- Braden, S. E., Stopar, J. D., Robinson, M. S., Lawrence, S. J., Van Der Bogert, C. H., & Hiesinger, H. (2014). Evidence for basaltic volcanism on the Moon within the past 100 million years. *Nature Geoscience*, 7(11), 787–791. <https://doi.org/10.1038/ngeo2252>
- Byrne, P. K., Klimczak, C., McGovern, P. J., Mazarico, E., James, P. B., Neumann, G. A., et al. (2015). Deep-seated thrust faults bound the Mare Crisium lunar mascon. *Earth and Planetary Science Letters*, 427, 183–190. <https://doi.org/10.1016/j.epsl.2015.06.022>
- Clark, J. D., Hurtado, J. M., Hiesinger, H., van der Bogert, C. H., & Bernhardt, H. (2017). Investigation of newly discovered lobate scarps: Implications for the tectonic and thermal evolution of the Moon. *Icarus*, 298, 78–88. <https://doi.org/10.1016/j.icarus.2017.08.017>
- Clark, J. D., Van Der Bogert, C. H., Hiesinger, H., Watters, T. R., & Robinson, M. S. (2019). Fault slip movement along wrinkle ridge-lobate scarp transitions in the last 100 Ma. In *50th lunar and planetary science conference*. Abstract #2084.
- Daket, Y., Yamaji, A., Sato, K., Haruyama, J., Morota, T., Ohtake, M., & Matsunaga, T. (2016). Tectonic evolution of northwestern Imbrium of the Moon that lasted in the Copernican period. *Earth Planets and Space*, 68(1), 157. <https://doi.org/10.1186/s40623-016-0531-0>
- De Hon, R. A. (1974). Thickness of mare material in the Tranquillitatis and Nectaris basins. In *5th lunar and planetary science conference* (Vol. 53–59).
- De Hon, R. A. (2017). A two-basin model for Mare Tranquillitatis. In *48th lunar and planetary science conference*. Abstract #2769.
- Dvorak, J., & Phillips, R. J. (1979). Gravity anomaly and structure associated with the Lamont region of the Moon. In *10th lunar and planetary science conference* (pp. 2265–2275).
- Elder, C. M., Haber, J., Hayne, P. O., Ghent, R. R., Williams, J.-P., & Siegler, M. A. (2022). Inferring lunar Mare basalt material properties from surface rock abundance. In *53rd lunar and planetary science conference*. Abstract #2360.
- Fagin, S. W., Worrall, D. M., & Muehlberger, W. R. (1978). Lunar mare ridge orientations: Implications for lunar tectonic models. In *9th lunar and planetary science conference* (pp. 3473–3479).
- Fassett, C. I., & Thomson, B. J. (2014). Crater degradation on the lunar Maria: Topographic diffusion and the rate of erosion on the Moon. *Journal of Geophysical Research: Planets*, 119(10), 2255–2271. <https://doi.org/10.1002/2014JE004698>
- Freed, A. M., Melosh, H. J., & Solomon, S. C. (2001). Tectonics of mascon loading: Resolution of the strike-slip faulting paradox. *Journal of Geophysical Research*, 106(E9), 20603–20620. <https://doi.org/10.1029/2000JE001347>
- French, R. A., Bina, C. R., Robinson, M. S., & Watters, T. R. (2015). Small-scale lunar graben: Distribution, dimensions, and formation processes. *Icarus*, 252, 95–106. <https://doi.org/10.1016/j.icarus.2014.12.031>
- French, R. A., Watters, T. R., & Robinson, M. S. (2019). Provenance of block fields along lunar wrinkle ridges. *Journal of Geophysical Research: Planets*, 124(11), 2970–2982. <https://doi.org/10.1029/2019JE006018>
- Frueh, T., Hiesinger, H., van der Bogert, C. H., Clark, J. D., Watters, T. R., & Schmedemann, N. (2023). Tectonic map and compressional feature Map of Mare Tranquillitatis, Moon (Version\_1) [Dataset]. Zenodo. <https://doi.org/10.5281/zenodo.7551409>
- Frueh, T., van der Bogert, C. H., Hiesinger, H., & Schmedemann, N. (2020). Reassessment of individual lunar wrinkle ridge ages in Mare Tranquillitatis. In *51st lunar and planetary science conference*. Abstract #1854.
- Fuqua Haviland, H., Weber, R. C., Neal, C. R., Lognonné, P., Garcia, R. F., Schmerr, N., et al. (2022). The lunar geophysical network landing sites science rationale. *The Planetary Science Journal*, 3(2), 40. <https://doi.org/10.3847/psj/ac0f82>
- Ghent, R. R., Hayne, P. O., Bandfield, J. L., Campbell, B. A., Allen, C. C., Carter, L. M., & Paige, D. A. (2014). Constraints on the recent rate of lunar ejecta breakdown and implications for crater ages. *Geology*, 42(12), 1059–1062. <https://doi.org/10.1130/G35926.1>
- Gold, T. (1972). Erosion, transportation and the nature of the Maria. In S. K. Runcorn, & H. C. Urey (Eds.), *The Moon*. International Astronomical Union/Union. (Vol. 47, pp. 55–67). <https://doi.org/10.1017/S0074180900097424>
- Golombek, M. P., Plescia, J. B., & Franklin, B. J. (1991). Faulting and folding in the formation of planetary wrinkle ridges. *Proceedings of Lunar and Planetary Science*, 21, 679–693.
- Hiesinger, H., Head, J. W., Wolf, U., Jaumann, R., & Neukum, G. (2011). Ages and stratigraphy of lunar mare basalts: A synthesis. In *Recent advances and current research issues in lunar stratigraphy* (Vol. 477, pp. 1–51). Geological Society of America Special Paper. <https://doi.org/10.1130/2011.2477/01>
- Hiesinger, H., Jaumann, R., Neukum, G., & Head, J. W. (2000). Ages of mare basalts on the lunar nearside. *Journal of Geophysical Research*, 105(E12), 29239–29275. <https://doi.org/10.1029/2000JE001244>
- Ikedo, A., Kumagai, H., & Morota, T. (2022). Topographic degradation processes of lunar crater walls inferred from boulder falls. *Journal of Geophysical Research: Planets*, 127(10), e2021JE007176. <https://doi.org/10.1029/2021je007176>
- Iqbal, W., Hiesinger, H., & van der Bogert, C. H. (2019). Geological mapping and chronology of lunar landing sites: Apollo 11. *Icarus*, 333, 528–547. <https://doi.org/10.1016/j.icarus.2019.06.020>
- Kahan, D. S. (2013). GRAIL Moon LGRS derived gravity science data products V1.0, GRAIL-L-LGRS-5-RDR-V1.0 [Dataset]. NASA Planetary Data System. <https://doi.org/10.17189/1519529>
- Konopliv, A. S., Asmar, S. W., Carranza, E., Sjogren, W. L., & Yuan, D. N. (2001). Recent gravity models as a result of the Lunar Prospector mission. *Icarus*, 150(1), 1–18. <https://doi.org/10.1006/icar.2000.6573>
- Lu, Y., Wu, Y., Michael, G. G., Basilevsky, A. T., & Li, C. (2019). Young wrinkle ridges in Mare Imbrium: Evidence for very recent compressional tectonism. *Icarus*, 329, 24–33. <https://doi.org/10.1016/j.icarus.2019.03.029>
- Lucchitta, B. K. (1976). Mare ridges and related highland scarps-Result of vertical tectonism? In *7th lunar and planetary science conference* (pp. 2761–2782).
- Lucchitta, B. K., & Watkins, J. A. (1978). Age of graben systems on the moon. In *9th lunar and planetary science conference* (pp. 3459–3472).
- Matsuyama, I., Keane, J. T., Trinh, A., Beuthe, M., & Watters, T. R. (2021). Global tectonic patterns of the Moon. *Icarus*, 358, 114202. <https://doi.org/10.1016/j.icarus.2020.114202>
- McGovern, P. J., Kramer, G. Y., & Neumann, G. A. (2022). Delayed onset of wrinkle ridge formation in Mare Tranquillitatis: A manifestation of lunar thermo-chemical evolution. In *53rd lunar and planetary science conference*. Abstract #2853.
- Montési, L. G. J., & Zuber, M. T. (2003). Clues to the lithospheric structure of Mars from wrinkle ridge sets and localization instability. *Journal of Geophysical Research*, 108(E6), 5048. <https://doi.org/10.1029/2002je001974>
- Muller, P. M., & Sjogren, W. L. (1968). Mascons: Lunar mass concentrations. *Science*, 161(3842), 680–684. <https://doi.org/10.1126/science.161.3842.680>
- Nelson, D. M., Koeber, S. D., Daud, K., Robinson, M. S., Watters, T. R., Banks, M. E., & Williams, N. R. (2014). Mapping lunar Maria extents and lobate scarps using LROC image products. In *45th lunar and planetary science conference*. Abstract #2861.
- Neumann, G. A. (2009). Lunar orbiter laser altimeter raw data set, LRO-L-LOLA-4-GDR-V1.0 [Dataset]. NASA Planetary Data System. <https://doi.org/10.17189/1520642>

- Nypaver, C. A., & Thomson, B. J. (2022). New observations of recently active wrinkle ridges in the lunar mare: Implications for the timing and origin of lunar tectonics. *Geophysical Research Letters*, *49*(17), e2022GL098975. <https://doi.org/10.1029/2022GL098975>
- Ohtake, M., Haruyama, J., Matsunaga, T., Yokota, Y., Morota, T., & Honda, C. (2008). Performance and scientific objectives of the SELENE (KAGUYA) multiband imager. *Earth Planets and Space*, *60*(4), 257–264. <https://doi.org/10.1186/BF03352789>
- Okubo, C. H., & Schultz, R. A. (2003). Two-dimensional wrinkle ridge strain & energy release based on numerical modeling of MOLA topography. In *34th lunar and planetary science conference*. Abstract #1283.
- Okubo, C. H., & Schultz, R. A. (2004). Mechanical stratigraphy in the western equatorial region of Mars based on thrust fault-related fold topography and implications for near-surface volatile reservoirs. *Bulletin of the Geological Society of America*, *116*(5/6), 594–605. <https://doi.org/10.1130/B25361.1>
- Ono, T., Kumamoto, A., Nakagawa, H., Yamaguchi, Y., Oshigami, S., Yamaji, A., et al. (2009). Lunar radar sounder observations of subsurface layers under the nearside Maria of the moon. *Science*, *323*(5916), 909–912. <https://doi.org/10.1126/science.1165988>
- Plescia, J. B., & Golombek, M. P. (1986). Origin of planetary wrinkle ridges based on the study of terrestrial analogs. *Bulletin of the Geological Society of America*, *97*(11), 1289–1299. [https://doi.org/10.1130/0016-7606\(1986\)97<1289:oopwrb>2.0.co;2](https://doi.org/10.1130/0016-7606(1986)97<1289:oopwrb>2.0.co;2)
- Qiao, L., Head, J. W., Wilson, L., & Ling, Z. (2020). The Cauchy 5 small, low-volume lunar shield volcano: Evidence for volatile exsolution-eruption patterns and type 1/type 2 hybrid irregular Mare patch formation. *Journal of Geophysical Research: Planets*, *125*, 1–28. <https://doi.org/10.1029/2019JE006171>
- Robinson, M. (2009). LRO Moon LROC 5 RDR V1.0 [Dataset]. NASA Planetary Data System (PDS). <https://doi.org/10.17189/1520341>
- Robinson, M. S., Speyerer, E. J., Boyd, A., Waller, D., Wagner, R. V., & Burns, K. N. (2012). Exploring the Moon with the lunar reconnaissance orbiter camera. *ISPRS - International Archives of the Photogrammetry, Remote Sensing and Spatial Information Sciences*, *XXXIX*, 501–504. <https://doi.org/10.5194/isprsarchives-xxxix-b4-501-2012>
- Schleicher, L. S., Watters, T. R., Martin, A. J., & Banks, M. E. (2019). Wrinkle ridges on Mercury and the Moon within and outside of mascons. *Icarus*, *331*, 226–237. <https://doi.org/10.1016/j.icarus.2019.04.013>
- Schultz, P. H., & Crawford, D. A. (2011). Origin of nearside structural and geochemical anomalies on the Moon. In *Recent advances and current research issues in lunar stratigraphy* (Vol. 477, pp. 141–159). Geological Society of America Special Paper. [https://doi.org/10.1130/2011.2477\(07](https://doi.org/10.1130/2011.2477(07)
- Schultz, R. A. (2000). Localization of bedding plane slip and backthrust faults above blind thrust faults: Keys to wrinkle ridge structure. *Journal of Geophysical Research E: Planets*, *105*(E5), 12035–12052. <https://doi.org/10.1029/1999JE001212>
- Scott, D. H. (1974). The geologic significance of some lunar gravity anomalies. In *5th lunar and planetary science conference* (pp. 3025–3036).
- Senthil Kumar, P., Sruthi, U., Krishna, N., Lakshmi, K. J. P., Menon, R., Amitabh, et al. (2016). Recent shallow moonquake and impact-triggered boulder falls on the Moon: New insights from the Schrödinger basin. *Journal of Geophysical Research: Planets*, *121*(2), 147–179. <https://doi.org/10.1002/2015JE004850>
- Sharpton, V. L., & Head, J. W. (1988). Lunar Mare ridges: Analysis of ridge-crater intersections and implications for the tectonic origin of Mare ridges. *18th Lunar and Planetary Science Conference*, 307–317.
- Solomon, S. C. (1986). On the early thermal state of the Moon. In *Origin of the Moon* (pp. 435–452). Lunar and Planetary Institute.
- Solomon, S. C., & Head, J. W. (1979). Vertical movement in mare basins: Relation to mare emplacement, basin tectonics, and lunar thermal history. *Journal of Geophysical Research*, *84*(B4), 1667–1682. <https://doi.org/10.1029/jb084ib04p01667>
- Spudis, P. D. (1993). From crater to basin. In *The geology of multi-ring impact basins* (Vol. 18–41). Cambridge University Press. <https://doi.org/10.1017/cbo9780511564581.003>
- Spudis, P. D., McGovern, P. J., & Kiefer, W. S. (2013). Large shield volcanoes on the Moon. *Journal of Geophysical Research: Planets*, *118*(5), 1063–1081. <https://doi.org/10.1002/jgre.20059>
- Strom, R. G. (1972). Lunar mare ridges, rings and volcanic ring complexes. In S. K. Runcorn & H. C. Urey (Eds.), *The Moon* (Vol. 47, pp. 187–215). International Astronomical Union. [https://doi.org/10.1007/978-94-010-2861-5\\_19](https://doi.org/10.1007/978-94-010-2861-5_19)
- Tian, H. C., Wang, H., Chen, Y., Yang, W., Zhou, Q., Zhang, C., et al. (2021). Non-KREEP origin for chang'e-5 basalts in the Procellarum KREEP Terrane. *Nature*, *600*(7887), 59–63. <https://doi.org/10.1038/s41586-021-04119-5>
- Trask, N. J. (1971). Geologic comparison of mare materials in the lunar equatorial belt, including Apollo 11 and Apollo 12 landing sites. *Geological Survey Research*, *750*, 138–144.
- Valantinas, A., Kinch, K. M., & Bridžius, A. (2017). Rocky outcrops and low crater densities on lunar wrinkle ridges: Evidence for recent tectonic activity? *European Planetary Science Congress*, *11*. Abstract #961.
- Valantinas, A., Kinch, K. M., & Bridžius, A. (2018). Low crater frequencies and low model ages in lunar Maria: Recent endogenic activity or degradation effects? *Meteoritics & Planetary Science*, *53*(4), 826–838. <https://doi.org/10.1111/maps.13033>
- Valantinas, A., & Schultz, P. H. (2020). The origin of neotectonics on the lunar nearside. *Geology*, *48*(7), 649–653. <https://doi.org/10.1130/g47202.1>
- van der Bogert, C. H., Clark, J. D., Hiesinger, H., Banks, M. E., Watters, T. R., & Robinson, M. S. (2018). How old are lunar lobate scarps? 1. Seismic resetting of crater size-frequency distributions. *Icarus*, *306*, 225–242. <https://doi.org/10.1016/j.icarus.2018.01.019>
- Watters, T. R. (1988). Wrinkle ridge assemblages on the terrestrial planets. *Journal of Geophysical Research*, *93*(B9), 10236–10254. <https://doi.org/10.1029/jb093ib09p10236>
- Watters, T. R. (2004). Elastic dislocation modeling of wrinkle ridges on Mars. *Icarus*, *171*(2), 284–294. <https://doi.org/10.1016/j.icarus.2004.05.024>
- Watters, T. R. (2022). Lunar wrinkle ridges and the evolution of the nearside lithosphere. *Journal of Geophysical Research: Planets*, *127*(3), e2021JE007058. <https://doi.org/10.1029/2021je007058>
- Watters, T. R., & Johnson, C. (2009). Lunar tectonics. In T. R. Watters & R. Schultz (Eds.), *Planetary tectonics*. Cambridge University Press.
- Watters, T. R., Robinson, M. S., Banks, M. E., Tran, T., & Denevi, B. W. (2012). Recent extensional tectonics on the Moon revealed by the lunar reconnaissance orbiter camera. *Nature Geoscience*, *5*(3), 181–185. <https://doi.org/10.1038/ngeo1387>
- Watters, T. R., Robinson, M. S., Beyer, R. A., Banks, M. E., Bell, J. F., Pritchard, M. E., et al. (2010). Evidence of recent thrust faulting on the Moon revealed by the lunar reconnaissance orbiter camera. *Science*, *329*(5994), 936–940. <https://doi.org/10.1126/science.1189590>
- Watters, T. R., Robinson, M. S., Collins, G. C., Banks, M. E., Daud, K., Williams, N. R., & Selvens, M. M. (2015). Global thrust faulting on the Moon and the influence of tidal stresses. *Geology*, *43*(10), 851–854. <https://doi.org/10.1130/G37120.1>
- Watters, T. R., Weber, R. C., Collins, G. C., Howley, I. J., Schmerr, N. C., & Johnson, C. L. (2019). Shallow seismic activity and young thrust faults on the Moon. *Nature Geoscience*, *12*(6), 411–417. <https://doi.org/10.1038/s41561-019-0362-2>
- Whitaker, E. A. (1981). The lunar Procellarum basin. In P. H. Schultz & R. B. Merrill (Eds.), *Multi-ring basins: Formation and evolution, proceedings of the lunar planetary Science* (pp. 105–111). Pergamon Press.
- Wieczorek, M. A., & Phillips, R. J. (2000). The “Procellarum KREEP Terrane”: Implications for mare volcanism and lunar evolution. *Journal of Geophysical Research*, *105*(E8), 20417–20430. <https://doi.org/10.1029/1999je001092>

- Wilhelms, D., McCauley, J., & Trask, N. (1987). *The geological history of the Moon*. US Government Printing Office.
- Williams, N. R., Bell, J. F., Watters, T. R., Banks, M. E., Daud, K., & French, R. A. (2019). Evidence for recent and ancient faulting at Mare Frigoris and implications for lunar tectonic evolution. *Icarus*, *326*, 151–161. <https://doi.org/10.1016/j.icarus.2019.03.002>
- Williams, N. R., Watters, T. R., Pritchard, M. E., Banks, M. E., & Bell, J. F. (2013). Fault dislocation modeled structure of lobate scarps from Lunar Reconnaissance Orbiter Camera digital terrain models. *Journal of Geophysical Research: Planets*, *118*(2), 224–233. <https://doi.org/10.1002/jgre.20051>
- Yong Technology Inc. (2014). “GeoRose” [Software]. Yong Technology Inc. Retrieved from <http://www.yongtechnology.com/download/georose>
- Yue, Z., Michael, G. G., Di, K., & Liu, J. (2017). Global survey of lunar wrinkle ridge formation times. *Earth and Planetary Science Letters*, *477*, 14–20. <https://doi.org/10.1016/j.epsl.2017.07.048>
- Zhang, F., Zhu, M. H., Bugiolacchi, R., Huang, Q., Osinski, G. R., Xiao, L., & Zou, Y. L. (2018). Diversity of basaltic lunar volcanism associated with buried impact structures: Implications for intrusive and extrusive events. *Icarus*, *307*, 216–234. <https://doi.org/10.1016/j.icarus.2017.10.039>
- Zharkova, A. Y., Kreslavsky, M. A., Head, J. W., & Kokhanov, A. A. (2020). Regolith textures on Mercury: Comparison with the Moon. *Icarus*, *351*, 113945. <https://doi.org/10.1016/j.icarus.2020.113945>
- Zuber, M. T., Smith, D. E., Watkins, M. M., Asmar, S. W., Konopliv, A. S., Lemoine, F. G., et al. (2013). Gravity field of the moon from the gravity recovery and interior laboratory (GRAIL) mission. *Science*, *339*(6120), 668–671. <https://doi.org/10.1126/science.1231507>